February 2, 2008

Consistency of the Two Higgs Doublet Model and CP violation in top production at the LHC

Abdul Wahab El Kaffas[a], Wafaa Khater[b], Odd Magne Ogreid[c] and Per Osland[a]

[a] Department of Physics and Technology, University of Bergen, Postboks 7803, N-5020 Bergen, Norway

[b] Department of Physics, Birzeit University, Palestine

[c] Bergen University College, Bergen, Norway

Abstract

It is important to provide guidance on whether CP violation may be measurable in top-quark production at the Large Hadron Collider. The present work extends an earlier analysis of the non-supersymmetric Two-Higgs-Doublet Model in this respect, by allowing a more general potential. Also, a more comprehensive study of theoretical and experimental constraints on the model is presented. Vacuum stability, unitarity, direct searches and electroweak precision measurements severely constrain the model. We explore, at low $\tan\beta$, the allowed regions in the multidimensional parameter space that give a viable physical model. This exploration is focused on the parameter space of the neutral sector rotation matrix, which is closely related to the Yukawa couplings of interest. In most of the remaining allowed regions, the model violates CP. We present a quantitative discussion of a particular CP-violating observable. This would be measurable in semileptonically decaying top and antitop quarks produced at the LHC, provided the number of available events is of the order of a million.

1 Introduction

The Two-Higgs-Doublet Model (2HDM) is attractive as one of the simplest extensions of the Standard Model that admits additional CP violation [1–3]. This is an interesting possibility, given the unexplained baryon asymmetry of the Universe [4, 5], and the possibility of exploring relevant, new physics at the LHC [6]. In particular, the model can lead to CP violation in $t\bar{t}$ production, a process which has received considerable theoretical attention [7–9], since it will become possible to severely constrain or even measure it.

CP violation can be induced in $t\bar{t}$ production at the one-loop level, by the exchange of neutral Higgs bosons which are not eigenstates under CP. This effect is only large enough to be of experimental interest if the neutral Higgs bosons are reasonably light, and have strong couplings to the top quarks.

Within the 2HDM (II), where the top quark gets its mass from coupling to the Higgs field Φ_2 [10] (see sect. 3.5), the condition of having sizable $Ht\bar{t}$ couplings forces us to consider small values of $\tan\beta$. A first exploration of this limit was presented in [11]. In that paper, the general conditions for measurability of CP violation in $gg \to t\bar{t}$ at the LHC [8] were found to be satisfied in a certain region of the 2HDM parameter space. In addition to having small $\tan\beta$, in order to have a measurable signal with a realistic amount of data (of the order of a million $t\bar{t}$ events), it was found necessary that the lightest neutral Higgs boson be light, and that the spectrum not be approximately degenerate. In fact, it was found that in the most favourable observable considered, the effect would not reach the per mil level unless there is one and only one Higgs boson below the $t\bar{t}$ threshold, and that $\tan\beta$ is at most of order unity. We here extend the analysis of [11] to the more general case, allowing the most general quartic couplings in the potential.

At small $\tan\beta$, also certain Yukawa couplings to charged Higgs bosons are enhanced. Such couplings contribute to effects that are known experimentally to very high precision. In particular, at low $\tan\beta$ the B^0_d–$\bar{B}^0_d$ oscillation data and the effective $Zb\bar{b}$ coupling, measured via R_b [12, 13] severely constrain the model, whereas the $b \to s\gamma$ data [14] constrain it at low $M_{H^\pm}$. Furthermore, the high-precision measurement of the W and Z masses, as expressed via ρ [13] constrains the splitting of the Higgs mass spectrum. Unless

there are cancellations, the charged Higgs boson can not be very much heavier than the lightest neutral one, and the lightest neutral one can not be far away from the mass scale of the W and the Z [15]. Also, the lightest one is constrained by the direct searches at LEP [16, 17]. We shall here study the interplay of these constraints, and estimate the amount of CP violation that may be measurable at the LHC in selected favorable regions of the remaining parameter space.

An important characteristic of the 2HDM (as opposed to the MSSM [18–22]) is the fact that, at the level of the mathematics, the masses of the neutral and the charged Higgs bosons are rather independent (see sect. 2). However, the experimental precision on $\Delta\rho$ (see sect. 4.3) forces the charged Higgs mass to be comparable in magnitude to the neutral Higgs masses. Another important difference is that whereas small values of $\tan\beta$ are practically excluded in the MSSM [23], in the 2HDM, which has more free parameters, they are not.

For a recent comprehensive discussion of the experimental constraints on the 2HDM (though mostly restricted to the CP-conserving limit), see [24] and [25]. The latter study, which considers the CP-conserving limit, concludes that the model is practically excluded, with the muon anomalous moment being very constraining. However, the interpretation of the data is now considered less firm, and furthermore, that study focuses on large $\tan\beta$, and is thus less relevant for the present work.

We present in sect. 2 an overview of the 2HDM, with focus on the approach of ref. [11], and outline the present extensions. In sect. 3 we discuss the model in more detail, in particular the implications of stability and unitarity, and review the conditions for having CP violation. In sect. 4 we discuss various experimental constraints on the model, with particular attention to small values of $\tan\beta$. In sect. 5 we present an overview of allowed parameter regions, also restricted to small $\tan\beta$. In sect. 6 we discuss the implications of the model for a particular CP-violating observable involving the energies of positrons and electrons from the decays of t and $\bar{t}$ produced in gluon–gluon collisions at the LHC. Sect. 7 contains a summary and conclusions.

2 Review of the Two-Higgs-Doublet Model

The 2HDM may be seen as an unconstrained version of the Higgs sector of the MSSM. While at tree level the latter can be parametrized in terms of only two parameters, conventionally taken to be $\tan\beta$ and M_A, the 2HDM has much more freedom. In particular, the neutral and charged Higgs masses are rather independent.

Traditionally, the 2HDM is defined in terms of the potential. The parameters of the potential (quartic and quadratic couplings) determine the masses of the neutral and the charged Higgs bosons. Alternatively, and this is the approach followed here and in ref. [11], one can take masses and mixing angles as input, and determine parameters of the potential as derived quantities. This approach highlights the fact that the neutral and charged sectors are rather independent, as well as masses being physically more accessible than quartic couplings. However, some choices of input will lead to physically acceptable potentials, others will not. This way, the two sectors remain correlated.

In addition, the 2HDM neutral sector may or may not lead to CP violation, depending on the choice of potential. We shall here consider the so-called Model II, where u-type quarks acquire masses from a Yukawa coupling to one Higgs doublet, Φ_2, whereas the d-type quarks couple to the other, Φ_1. This structure is the same as in the MSSM.

2.1 The approach of ref. [11]

The amount of CP violation that can be measured in $t\bar{t}$ production was related to the Higgs mass spectrum and other model parameters in [11]. In that paper, the Higgs potential studied was parametrized as [26]

$$\begin{aligned} V &= \frac{\lambda_1}{2}(\Phi_1^\dagger\Phi_1)^2 + \frac{\lambda_2}{2}(\Phi_2^\dagger\Phi_2)^2 + \lambda_3(\Phi_1^\dagger\Phi_1)(\Phi_2^\dagger\Phi_2) + \lambda_4(\Phi_1^\dagger\Phi_2)(\Phi_2^\dagger\Phi_1) \\ &\quad + \frac{1}{2}\left[\lambda_5(\Phi_1^\dagger\Phi_2)^2 + \text{h.c.}\right] \\ &\quad - \frac{1}{2}\left\{m_{11}^2(\Phi_1^\dagger\Phi_1) + \left[m_{12}^2(\Phi_1^\dagger\Phi_2) + \text{h.c.}\right] + m_{22}^2(\Phi_2^\dagger\Phi_2)\right\}. \end{aligned} \tag{2.1}$$

Expanding the Higgs-doublet fields as

$$\Phi_i = \begin{pmatrix} \varphi_i^+ \\ \frac{1}{\sqrt{2}}(v_i + \eta_i + i\chi_i) \end{pmatrix} \tag{2.2}$$

and choosing phases of Φ_i such that v_1 and v_2 are both real [27], it is convenient to define $\eta_3 = -\sin\beta\chi_1 + \cos\beta\chi_2$ orthogonal to the neutral Goldstone boson $G^0 = \cos\beta\chi_1 + \sin\beta\chi_2$. In the basis $(\eta_1,\ \eta_2,\ \eta_3)$, the resulting mass-squared matrix $\mathcal{M}^2$ of the neutral sector, can then be diagonalized to physical states $(H_1,\ H_2,\ H_3)$ with masses $M_1 \leq M_2 \leq M_3$, via a rotation matrix R:

$$\begin{pmatrix} H_1 \\ H_2 \\ H_3 \end{pmatrix} = R \begin{pmatrix} \eta_1 \\ \eta_2 \\ \eta_3 \end{pmatrix}, \tag{2.3}$$

satisfying

$$R\mathcal{M}^2 R^{\mathrm{T}} = \mathcal{M}^2_{\mathrm{diag}} = \mathrm{diag}(M_1^2, M_2^2, M_3^2), \tag{2.4}$$

and parametrized as[1]

$$\begin{aligned} R = R_3\, R_2\, R_1 &= \begin{pmatrix} 1 & 0 & 0 \\ 0 & \cos\alpha_3 & \sin\alpha_3 \\ 0 & -\sin\alpha_3 & \cos\alpha_3 \end{pmatrix} \begin{pmatrix} \cos\alpha_2 & 0 & \sin\alpha_2 \\ 0 & 1 & 0 \\ -\sin\alpha_2 & 0 & \cos\alpha_2 \end{pmatrix} \begin{pmatrix} \cos\alpha_1 & \sin\alpha_1 & 0 \\ -\sin\alpha_1 & \cos\alpha_1 & 0 \\ 0 & 0 & 1 \end{pmatrix} \\ &= \begin{pmatrix} c_1\, c_2 & s_1\, c_2 & s_2 \\ -(c_1\, s_2\, s_3 + s_1\, c_3) & c_1\, c_3 - s_1\, s_2\, s_3 & c_2\, s_3 \\ -c_1\, s_2\, c_3 + s_1\, s_3 & -(c_1\, s_3 + s_1\, s_2\, c_3) & c_2\, c_3 \end{pmatrix} \end{aligned} \tag{2.5}$$

with $c_i = \cos\alpha_i$, $s_i = \sin\alpha_i$. The rotation angle α_1 is chosen such that in the limit of no CP violation ($s_2 \to 0$, $s_3 \to 0$) then $\alpha_1 \to \alpha + \frac{1}{2}\pi$, where α is the familiar mixing angle of the CP-even sector, and the additional $\frac{1}{2}\pi$ provides the mapping $H_1 \leftrightarrow h$, instead of H being in the $(1,1)$ position of $\mathcal{M}^2_{\mathrm{diag}}$, as is used in the MSSM [10].

While the signs of η_i and χ_i are fixed by our choice of taking the vacuum expectation values real and positive [27], the phase of H_i has no physical consequence. One may therefore freely change the sign of one or more rows, e.g., let $R_{1i} \to -R_{1i}$ (see sect. 3.1.1).

Rather than describing the phenomenology in terms of the parameters of the potential (2.1), in [11] the physical mass of the charged Higgs boson, as well as those of the two lightest neutral ones, were taken as input, together with the rotation matrix R. Thus, the input can be summarized as

$$\text{Parameters: } \tan\beta,\ (M_1,\ M_2),\ (M_{H^\pm},\ \mu^2),\ (\alpha_1,\ \alpha_2,\ \alpha_3), \tag{2.6}$$

where $\tan\beta = v_2/v_1$ and $\mu^2 = v^2\nu$, with $\nu = \mathrm{Re}\, m_{12}^2/(2v_1v_2)$ and $v = 246$ GeV.

[1] In ref. [11], these angles were referred to as $(\tilde{\alpha}, \alpha_b, \alpha_c) \leftrightarrow (\alpha_1, \alpha_2, \alpha_3)$.

This approach provides better control of the physical content of the model. In particular, the elements R_{13} and R_{23} of the rotation matrix must be non-zero in order to yield CP violation. For consistency, this requires $\mathrm{Im}\,\lambda_5$ and $\mathrm{Im}\,m_{12}^2$ (as derived quantities) to be non-zero.

2.2 The general potential

For the potential, in this study, we take

$$V = \text{Expression (2.1)} + \left\{ \left[\lambda_6 (\Phi_1^\dagger \Phi_1) + \lambda_7 (\Phi_2^\dagger \Phi_2) \right] (\Phi_1^\dagger \Phi_2) + \text{h.c.} \right\}. \tag{2.7}$$

The new terms proportional to λ_6 and λ_7 have to be carefully constrained, since this potential does not satisfy natural flavour conservation [28], even if each doublet is coupled only to up-type or only to down-type flavours.

The various coupling constants in the potential will of course depend on the choice of basis (Φ_1, Φ_2). Recently, there has been some focus [29] on the importance of formulating physical observables in a basis-independent manner. Here, we shall adopt the so-called Model II [10] for the Yukawa couplings. This will uniquely identify the basis in the (Φ_1, Φ_2) space.

Minimizing the potential (2.7), we can rewrite it (modulo a constant) as

$$\begin{aligned} V &= \frac{\lambda_1}{2} \left[(\Phi_1^\dagger \Phi_1) - \frac{v_1^2}{2} \right]^2 + \frac{\lambda_2}{2} \left[(\Phi_2^\dagger \Phi_2) - \frac{v_2^2}{2} \right]^2 + \lambda_3 (\Phi_1^\dagger \Phi_1)(\Phi_2^\dagger \Phi_2) + \lambda_4 (\Phi_1^\dagger \Phi_2)(\Phi_2^\dagger \Phi_1) \\ &\quad + \left\{ \frac{1}{2} \lambda_5 (\Phi_1^\dagger \Phi_2)^2 + \left[\lambda_6 (\Phi_1^\dagger \Phi_1) + \lambda_7 (\Phi_2^\dagger \Phi_2) \right] (\Phi_1^\dagger \Phi_2) + \text{h.c.} \right\} \\ &\quad - \frac{1}{2} \left[\mathrm{Re}\,\lambda_{34567} - 2\nu \right] \left[v_2^2 (\Phi_1^\dagger \Phi_1) + v_1^2 (\Phi_2^\dagger \Phi_2) \right] - v_1 v_2\, \mathrm{Re} \left[\lambda_6 (\Phi_1^\dagger \Phi_1) + \lambda_7 (\Phi_2^\dagger \Phi_2) \right] \\ &\quad - v_1 v_2 \left[2\nu\, \mathrm{Re}\,(\Phi_1^\dagger \Phi_2) - \mathrm{Im}\,\lambda_{567}\, \mathrm{Im}\,(\Phi_1^\dagger \Phi_2) \right]. \end{aligned} \tag{2.8}$$

Here and in the following, we adopt the abbreviations

$$\lambda_{345} = \lambda_3 + \lambda_4 + \lambda_5, \quad \lambda_{34567} = \lambda_{345} + \frac{v_1}{v_2}\,\lambda_6 + \frac{v_2}{v_1}\,\lambda_7, \quad \lambda_{567} = \lambda_5 + \frac{v_1}{v_2}\,\lambda_6 + \frac{v_2}{v_1}\,\lambda_7. \tag{2.9}$$

The mass-squared matrix $\mathcal{M}^2$ of (2.4), corresponding to the neutral sector of the potential, is found to be

$$\mathcal{M}_{11}^2 = v^2 [c_\beta^2\, \lambda_1 + s_\beta^2\, \nu + \frac{s_\beta}{2c_\beta} \mathrm{Re}\,(3c_\beta^2\, \lambda_6 - s_\beta^2\, \lambda_7)],$$

$$
\begin{aligned}
\mathcal{M}^2_{22} &= v^2[s^2_\beta\,\lambda_2 + c^2_\beta\,\nu + \frac{c_\beta}{2s_\beta}\mathrm{Re}\,(-c^2_\beta\,\lambda_6 + 3s^2_\beta\,\lambda_7)],\\
\mathcal{M}^2_{33} &= v^2\mathrm{Re}\,[-\lambda_5 + \nu - \frac{1}{2c_\beta s_\beta}(c^2_\beta\,\lambda_6 + s^2_\beta\,\lambda_7)],\\
\mathcal{M}^2_{12} &= v^2[c_\beta s_\beta(\mathrm{Re}\,\lambda_{345} - \nu) + \tfrac{3}{2}\mathrm{Re}\,(c^2_\beta\,\lambda_6 + s^2_\beta\,\lambda_7)],\\
\mathcal{M}^2_{13} &= -\tfrac{1}{2}v^2\mathrm{Im}\,[s_\beta\,\lambda_5 + 2c_\beta\,\lambda_6],\\
\mathcal{M}^2_{23} &= -\tfrac{1}{2}v^2\mathrm{Im}\,[c_\beta\,\lambda_5 + 2s_\beta\,\lambda_7],
\end{aligned}
\tag{2.10}
$$

with $\mathcal{M}^2_{ji} = \mathcal{M}^2_{ij}$.

Here, compared with the potential (2.1), we have two more complex parameters, λ_6 and λ_7 (four new real parameters), but rather than those, we take as additional parameters M_3, $\mathrm{Im}\,\lambda_5$, $\mathrm{Re}\,\lambda_6$ and $\mathrm{Re}\,\lambda_7$. Thus, the input will be

$$
\text{Parameters: } \tan\beta,\ (M_1,\ M_2,\ M_3),\ (M_{H^\pm},\ \mu^2),\ (\alpha_1,\ \alpha_2,\ \alpha_3),\ \mathrm{Im}\,\lambda_5,\ (\mathrm{Re}\,\lambda_6,\ \mathrm{Re}\,\lambda_7).
\tag{2.11}
$$

3 Model properties

We want to explore regions of parameter space where there is significant CP violation. In order to do that, we need to map out regions in the $\{\alpha_1, \alpha_2, \alpha_3\}$ space where the model is consistent (figures are presented in sect. 5).

From eq. (2.4), it follows that

$$
\mathcal{M}^2_{ij} = \sum_k R_{ki} M^2_k R_{kj}. \tag{3.1}
$$

Here, it is evident that the signs of the rows of R play no role.

Comparing the expressions (3.1) with (2.10), invoking also

$$
M^2_{H^\pm} = \mu^2 - \tfrac{1}{2}v^2(\lambda_4 + \mathrm{Re}\ \lambda_{567}), \tag{3.2}
$$

we can solve for the λ's. In particular, it follows from (2.10) that

$$
\begin{aligned}
\mathrm{Im}\,\lambda_6 &= -\frac{1}{c_\beta}\left[\frac{1}{v^2}\mathcal{M}^2_{13} + \frac{s_\beta}{2}\mathrm{Im}\,\lambda_5\right],\\
\mathrm{Im}\,\lambda_7 &= -\frac{1}{s_\beta}\left[\frac{1}{v^2}\mathcal{M}^2_{23} + \frac{c_\beta}{2}\mathrm{Im}\,\lambda_5\right].
\end{aligned}
\tag{3.3}
$$

3.1 Symmetries

By exploiting certain symmetries of the rotation matrix R, we can reduce the ranges of parameters that have to be explored.

3.1.1 Transformations of the rotation matrix

The rotation matrix R is invariant under the following transformation;

$$\text{A}: \quad \alpha_1 \to \pi + \alpha_1,\ \alpha_2 \to \pi - \alpha_2,\ \alpha_3 \to \pi + \alpha_3; \tag{3.4}$$

which leaves its elements unchanged.

Another class of transformations are those where two rows of R (i.e., physical Higgs fields) change sign, as discussed in sect. 2.1. The transformations are [11]:

$$\begin{aligned}
&\text{B1}: \quad \alpha_1 \to \pi + \alpha_1,\ \alpha_2 \to \pi - \alpha_2,\ \alpha_3 \text{ fixed}: && R_{1i} \to R_{1i}, && R_{2i} \to -R_{2i}, && R_{3i} \to -R_{3i},\\
&\text{B2}: \quad \alpha_1 \text{ fixed},\ \alpha_2 \to \pi + \alpha_2,\ \alpha_3 \to -\alpha_3: && R_{1i} \to -R_{1i}, && R_{2i} \to R_{2i}, && R_{3i} \to -R_{3i},\\
&\text{B3}: \quad \alpha_1 \to \pi + \alpha_1,\ \alpha_2 \to -\alpha_2,\ \alpha_3 \to -\alpha_3: && R_{1i} \to -R_{1i}, && R_{2i} \to -R_{2i}, && R_{3i} \to R_{3i}.
\end{aligned} \tag{3.5}$$

Actually, any one of these is a combination of the other two. For example, the transformation B3 is the combination of B1 and B2. Other transformations exist that will yield the same symmetries, but they will be combinations of one of these three transformations followed by the transformation A. In total we have 6 different transformations that yield symmetries of type B.

The third class of transformation we consider are those where two columns of R change sign. These transformations are:

$$\begin{aligned}
&\text{C1}: \quad \alpha_1 \to \pi - \alpha_1,\ \alpha_2 \to \pi + \alpha_2,\ \alpha_3 \text{ fixed}: && R_{j1} \to R_{j1}, && R_{j2} \to -R_{j2}, && R_{j3} \to -R_{j3},\\
&\text{C2}: \quad \alpha_1 \to -\alpha_1,\ \alpha_2 \to \pi + \alpha_2,\ \alpha_3 \text{ fixed}: && R_{j1} \to -R_{j1}, && R_{j2} \to R_{j2}, && R_{j3} \to -R_{j3},\\
&\text{C3}: \quad \alpha_1 \to \pi + \alpha_1,\ \alpha_2 \text{ fixed},\ \alpha_3 \text{ fixed}: && R_{j1} \to -R_{j1}, && R_{j2} \to -R_{j2}, && R_{j3} \to R_{j3}.
\end{aligned} \tag{3.6}$$

The transformation C3 is the combination of the transformations C1 and C2. Other transformations exist that will yield the same symmetries, but they will be combinations

of one of these three transformations followed by the transformation A. In total we have 6 different transformation that yield symmetries of type C.

Under transformations of type A and B, the resulting mass-squared matrix $\mathcal{M}^2 = R^T \mathcal{M}^2_{\text{diag}} R$ will be invariant. We make use of this fact along with the symmetries A, B1 and B2 to reduce the parameter space under consideration to

$$-\pi/2 < \{\alpha_1, \alpha_2, \alpha_3\} \leq \pi/2. \tag{3.7}$$

Under transformations of type C, the mass-squared matrix will not be invariant, some of its non-diagonal elements will change sign while the rest are unaltered.

$$\begin{aligned}
&\text{C1}: \quad \mathcal{M}^2_{12} \to -\mathcal{M}^2_{12}, \quad \mathcal{M}^2_{13} \to -\mathcal{M}^2_{13}, \quad \mathcal{M}^2_{23} \to +\mathcal{M}^2_{23}, \\
&\text{C2}: \quad \mathcal{M}^2_{12} \to -\mathcal{M}^2_{12}, \quad \mathcal{M}^2_{13} \to +\mathcal{M}^2_{13}, \quad \mathcal{M}^2_{23} \to -\mathcal{M}^2_{23}, \\
&\text{C3}: \quad \mathcal{M}^2_{12} \to +\mathcal{M}^2_{12}, \quad \mathcal{M}^2_{13} \to -\mathcal{M}^2_{13}, \quad \mathcal{M}^2_{23} \to -\mathcal{M}^2_{23}.
\end{aligned} \tag{3.8}$$

While a change of the sign of $\mathcal{M}^2_{12}$ implies changes in the physical content of the model, a change of sign of $\mathcal{M}^2_{13}$ and/or $\mathcal{M}^2_{23}$ can be compensated for by adjusting the imaginary parts of λ_5, λ_6 and λ_7. Thus, the most interesting transformation among the set (3.8) is C3.

The transformation B3 $\cdot$ C3 is physically equivalent to C3 since transformations of type B leave the mass-squared matrix invariant:

$$\text{B3}\cdot\text{C3}: \quad \alpha_1 \text{ fixed}, \alpha_2 \to -\alpha_2, \ \alpha_3 \to -\alpha_3: \quad \mathcal{M}^2_{12} \to +\mathcal{M}^2_{12}, \quad \mathcal{M}^2_{13} \to -\mathcal{M}^2_{13}, \quad \mathcal{M}^2_{23} \to -\mathcal{M}^2_{23}. \tag{3.9}$$

When $\text{Im}\,\lambda_5 = 0$, it follows from (3.3) that a sign change of $\mathcal{M}^2_{13}$ and $\mathcal{M}^2_{23}$ can be compensated for by sign changes of $\text{Im}\,\lambda_6$ and $\text{Im}\,\lambda_7$. These signs play no role in the discussion of stability (see Appendix A) and unitarity [30]. We shall therefore, when discussing the case $\text{Im}\,\lambda_5 = 0$ (sects. 5.1 and 5.2), make use of (3.9) to restrict the angular range from (3.7) to the smaller

$$-\pi/2 < \{\alpha_1, \alpha_2\} \leq \pi/2, \quad 0 \leq \alpha_3 \leq \pi/2. \tag{3.10}$$

When $\text{Im}\,\lambda_5 \neq 0$ we need to consider the angular range as given in (3.7).

3.1.2 Inversion of $\tan\beta$

The Higgs sector is invariant under

$$\begin{aligned} \tan\beta &\leftrightarrow \cot\beta, \qquad & \alpha_1 &\leftrightarrow \tfrac{1}{2}\pi - \alpha_1, \\ \alpha_2 &\leftrightarrow -\alpha_2, \qquad & \alpha_3 &\leftrightarrow \alpha_3, \end{aligned} \tag{3.11}$$

accompanied by

$$\begin{aligned} \lambda_1 &\leftrightarrow \lambda_2, \qquad & \lambda_3, \lambda_4 &\leftrightarrow \lambda_3, \lambda_4, \\ \lambda_5 &\leftrightarrow \lambda_5^\star, \qquad & \lambda_6 &\leftrightarrow \lambda_7^\star. \end{aligned} \tag{3.12}$$

This is just the symmetry between Φ_1 and Φ_2, and will be violated by the introduction of Model II Yukawa couplings, which distinguish between the two Higgs doublets, i.e., between $\tan\beta$ and $\cot\beta$.

3.2 CP violation

In general, with all three rotation-matrix angles non-zero, the model will violate CP. However, in certain limits, this is not the case. In order *not* to have CP violation, the mass-squared matrix must be block diagonal, i.e., one must require

$$\mathcal{M}^2_{13} = \mathcal{M}^2_{23} = 0. \tag{3.13}$$

Thus, CP *conservation* requires

$$\begin{aligned} \mathcal{M}^2_{13} &= M_1^2 R_{11} R_{13} + M_2^2 R_{21} R_{23} + M_3^2 R_{31} R_{33} = 0, \\ \mathcal{M}^2_{23} &= M_1^2 R_{12} R_{13} + M_2^2 R_{22} R_{23} + M_3^2 R_{32} R_{33} = 0. \end{aligned} \tag{3.14}$$

One possible solution of (3.14) is that

$$M_1 = M_2 = M_3. \tag{3.15}$$

The expressions (3.14) then vanish, by the orthogonality of R. There are additional limits of no CP violation, as discussed below.

Expressed in terms of the angles of the rotation matrix, the above elements describing mixing of the CP-even and CP-odd parts of $\mathcal{M}^2$ take the form

$$\begin{aligned}\mathcal{M}^2_{13} &= c_1 c_2 s_2 (M_1^2 - s_3^2 M_2^2 - c_3^2 M_3^2) + s_1 c_2 c_3 s_3 (-M_2^2 + M_3^2), \\ \mathcal{M}^2_{23} &= c_1 c_2 c_3 s_3 (M_2^2 - M_3^2) + s_1 c_2 s_2 (M_1^2 - s_3^2 M_2^2 - c_3^2 M_3^2).\end{aligned} \tag{3.16}$$

In the mass-non-degenerate case, they vanish (there is thus no CP violation) if either:

$$\begin{aligned}&\text{Case I:} \quad \sin 2\alpha_2 = 0, \quad \text{and} \quad \sin 2\alpha_3 = 0, \quad \text{or} \\ &\text{Case II:} \quad \cos\alpha_2 = 0, \quad \alpha_3 \quad \text{arbitrary.}\end{aligned} \tag{3.17}$$

Note that $M_1^2 - s_3^2 M_2^2 - c_3^2 M_3^2 < 0$ for non-degenerate or partially degenerate masses, ordered such that $M_1 \leq M_2 \leq M_3$ (where no more than two of the masses are equal). Thus, there are no additional CP-conserving solutions for the vanishing of this factor. The cases of partial degeneracy, $M_1 = M_2 \neq M_3$, and $M_1 \neq M_2 = M_3$ will be discussed in sect. 3.7.

It is thus natural to focus on the angles α_2 and α_3. In particular, since $R_{12}R_{13}$ is associated with CP-violation in the $H_1 t\bar{t}$ coupling (see sect. 3.5), we are interested in regions where $|\sin(2\alpha_2)|$ is large.

3.3 Reference parameters

In order to search for parameters with "large" CP violation, we will assume H_1 is light, and that M_2 is not close to M_1, as such degeneracy would cancel any CP violation.

For illustration, as a conservative default set of parameters, we take

$$\text{Set A:} \quad \begin{cases} \tan\beta = \{0.5, 1.0, 2.0\}, \ (M_1, M_2, M_3) = (100, 300, 500) \text{ GeV}, \\ M_{H^\pm} = 500 \text{ GeV}, \ \mu^2 = (200 \text{ GeV})^2, \ \text{Im}\,\lambda_5 = 0, \ \text{Re}\,\lambda_6 = \text{Re}\,\lambda_7 = 0. \end{cases} \tag{3.18}$$

Here, the lightest neutral Higgs boson can be accommodated by the negative LEP searches [16, 17] provided it does not couple too strongly to the Z, and the charged Higgs boson mass is compatible with the negative LEP [13] and Fermilab searches [31] as well as with the B_d^0–$\bar{B}_d^0$ oscillation, R_b constraints [25] (see sect. 4.1) and the $b \to s\gamma$ analysis at low $\tan\beta$ [14].

As a second set of parameters, we take

$$\text{Set B:} \quad \begin{cases} \tan\beta = \{0.5, 1.0, 2.0\},\ (M_1, M_2) = (80, 300)\ \text{GeV},\ M_3 = \{400, 600\}\ \text{GeV} \\ M_{H^\pm} = 300\ \text{GeV},\ \mu^2 = \{0, (200\ \text{GeV})^2\},\ \text{Im}\,\lambda_5 = 0,\ \text{Re}\,\lambda_6 = \text{Re}\,\lambda_7 = 0. \end{cases} \tag{3.19}$$

This set, which represents a light Higgs sector, is marginally in conflict with data (the combination of charged-Higgs mass and $\tan\beta$ values violate the R_b constraints by up to 5σ, see Table 2 in sect. 4.5), but is chosen for a more "optimistic" comparison, since it could give more CP violation due to a lower value of M_1 (which enhances the loop integrals).

3.4 Stability and unitarity

A necessary condition we must impose on the model, is that the potential is positive when $|\Phi_1|$ and $|\Phi_2| \to \infty$. This constraint, which is rather involved, is discussed in Appendix A. Two obvious conditions are that

$$\lambda_1 > 0, \qquad \lambda_2 > 0. \tag{3.20}$$

In general, the additional stability constraint is that λ_3 and λ_4 cannot be "too large and negative", and that $|\lambda_5|$, $|\lambda_6|$, $|\lambda_7|$ cannot be "too large".

Furthermore, we shall impose tree-level unitarity on the Higgs-Higgs-scattering sector, as formulated in [30, 32] (see also ref. [33]). This latter constraint is related to the perturbativity constraint (λ's not allowed "too large") adopted in ref. [11], but actually turns out to be numerically more severe.

3.5 Yukawa couplings

With the above notation, and adopting the so-called Model II [10] for the Yukawa couplings, where the down-type and up-type quarks are coupled only to Φ_1 and Φ_2, respectively, the couplings can be expressed (relative to the SM coupling) as

$$\begin{aligned} H_j b\bar{b}: &\qquad \frac{1}{\cos\beta}\,[R_{j1} - i\gamma_5 \sin\beta R_{j3}], \\ H_j t\bar{t}: &\qquad \frac{1}{\sin\beta}\,[R_{j2} - i\gamma_5 \cos\beta R_{j3}] \equiv a + i\tilde{a}\gamma_5. \end{aligned} \tag{3.21}$$

Likewise, we have for the charged Higgs bosons [10]

$$H^+ b\bar{t}: \qquad \frac{ig}{2\sqrt{2}m_W}\,[m_b(1+\gamma_5)\tan\beta + m_t(1-\gamma_5)\cot\beta],$$
$$H^- t\bar{b}: \qquad \frac{ig}{2\sqrt{2}m_W}\,[m_b(1-\gamma_5)\tan\beta + m_t(1+\gamma_5)\cot\beta]. \tag{3.22}$$

With this Yukawa structure, the model is denoted as the 2HDM (II).

The product of the $H_j t\bar{t}$ scalar and pseudoscalar couplings,

$$\gamma_{CP}^{(j)} = -a\,\tilde{a} = \frac{\cos\beta}{\sin^2\beta}\,R_{j2}R_{j3} \tag{3.23}$$

plays an important role in determining the amount of CP violation in the top-quark sector.

As was seen in ref. [11], unless the Higgs boson is resonant with the $t\bar{t}$ system, CP violation is largest for small Higgs masses. For a first orientation, we shall therefore focus on the contributions of the lightest Higgs boson, H_1. (There will also be significant contributions from the two heavier Higgs bosons, as discussed in sect. 6.) For the lightest Higgs boson, the coupling (3.21) becomes

$$H_1 t\bar{t}: \qquad \frac{1}{\sin\beta}\,[\sin\alpha_1\cos\alpha_2 - i\gamma_5\cos\beta\sin\alpha_2], \quad \text{with} \quad \gamma_{CP}^{(1)} = \tfrac{1}{2}\,\frac{\sin\alpha_1\sin(2\alpha_2)}{\tan\beta\sin\beta}, \tag{3.24}$$

where α_1 and α_2 are mixing angles of the Higgs mass matrix as defined by Eqs. (2.4) and (2.5).

From (3.24), we see that low $\tan\beta$ are required for having large CP violation in the top-quark sector. However, according to (3.22), for low $\tan\beta$ the charged-Higgs Yukawa coupling is also enhanced. Thus, for low $\tan\beta$, the R_b, ΔM_{B_d} [12,13] and $b \to s\gamma$ constraints [14] force $M_{H^\pm}$ to be high. For a quantitative discussion, see sect. 4.1.

3.6 CP violation in the Yukawa sector

We shall in sect. 6 study CP violation in the process

$$pp \to t\bar{t}X \to e^+e^-X, \tag{3.25}$$

focusing on the sub-process

$$gg \to t\bar{t} \to e^+e^-X. \tag{3.26}$$

Let the CP violating quantity of that process be given by [8, 11]

$$\sum_{j=1}^{3} R_{j2}\, R_{j3}\, f(M_j), \tag{3.27}$$

where $f(M_j)$ is some function of the neutral Higgs mass M_j, in general determined by loop integrals.

When the three neutral Higgs bosons are light, they will *all* contribute to the CP-violating effects. In fact, in the limit of three mass-degenerate Higgs bosons, the model may still be consistent in the sense that solutions can be found in some regions of parameter space, but the CP violation will cancel, since [cf. eq. (3.23)]

$$\sum_{j=1}^{3} \gamma_{CP}^{(j)} = \frac{\cos\beta}{\sin^2\beta} \sum_{j=1}^{3} R_{j2}\, R_{j3} = 0 \tag{3.28}$$

due to the orthogonality of R.

3.7 Degenerate limits

The set of free parameters (2.11) permits all three neutral Higgs masses to be degenerate. As discussed above, in this limit there is no CP violation, by orthogonality of the rotation matrix R. However, in contrast to the case of $\lambda_6 = \lambda_7 = 0$ studied in [11], the partial degeneracies are non-trivial and may lead to CP violation for certain choices of the angles α_i:

$\boldsymbol{M_1 = M_2 \equiv m \neq M_3}$**.** In this limit, the elements of $\mathcal{M}^2$ that induce CP violation, are

$$\begin{aligned} \mathcal{M}^2_{13} &= R_{31}R_{33}(M_3^2 - m^2) = c_2c_3(s_1s_3 - c_1s_2c_3)(M_3^2 - m^2), \\ \mathcal{M}^2_{23} &= R_{32}R_{33}(M_3^2 - m^2) = -c_2c_3(c_1s_3 + s_1s_2c_3)(M_3^2 - m^2). \end{aligned} \tag{3.29}$$

These both vanish, when the conditions (3.17) are satisfied, or else, when

$$\cos\alpha_3 = 0, \quad \alpha_1, \alpha_2 \quad \text{arbitrary}. \tag{3.30}$$

By orthogonality, when the two lighter Higgs bosons are degenerate, the CP violation (3.27) in the top-quark sector is proportional to

$$R_{32}\, R_{33}[f(M_3) - f(m)] \sim \mathcal{M}^2_{23}. \tag{3.31}$$

Thus, even though the model violates CP in the limit $M_1 = M_2 \neq M_3$, by for example having $\mathcal{M}^2_{13} \neq 0$, the top-quark sector would not violate CP at the one-loop level unless $\mathcal{M}^2_{23} \sim R_{32}R_{33} \neq 0$.

$\boldsymbol{M_1 \neq M_2 = M_3 \equiv M.}$ In this limit, the elements of $\mathcal{M}^2$ that induce CP violation are

$$\begin{aligned}\mathcal{M}^2_{13} &= -R_{11}R_{13}(M^2 - M_1^2) = -c_1c_2s_2(M^2 - M_1^2),\\ \mathcal{M}^2_{23} &= -R_{12}R_{13}(M^2 - M_1^2) = -s_1c_2s_2(M^2 - M_1^2).\end{aligned} \tag{3.32}$$

We note that these both vanish for $\sin(2\alpha_2) = 0$, meaning $\alpha_2 = 0$ or $\alpha_2 = \pi/2$. Thus, in the limit $M_1 \neq M_2 = M_3$ and $\alpha_2 = 0$, but α_3 *arbitrary*, the model does *not* violate CP, in agreement with the results of [11].

In this limit of the two heavier Higgs bosons being degenerate, the CP violation in the top-quark sector is proportional to[2]

$$R_{12}\, R_{13}[f(M_1) - f(M)] \sim \mathcal{M}^2_{23}. \tag{3.33}$$

In our parametrization, this is non-zero for

$$\sin\alpha_1 \neq 0, \quad \sin 2\alpha_2 \neq 0, \tag{3.34}$$

but with α_3 arbitrary.

In the more constrained model discussed in [11], the latter limits of only two masses being degenerate do not exist. In that case, with $\lambda_6 = \lambda_7 = 0$, a degeneracy of two masses forces the third one to have that same value.

4 Experimental model constraints at low $\tan\beta$

It is convenient to split the experimental constraints on the 2HDM into two categories. There are those involving only the charged Higgs boson, $H^\pm$, and those also involving the neutral ones. The former, like the non-discovery of a charged Higgs boson, the $b \to s\gamma$ constraint [14], and the B^0_d–$\bar{B}^0_d$ oscillations [25] do not depend on the rotation matrix R

[2]Whereas both these degenerate limits yield CP-violation in the t-quark sector proportional to $\mathcal{M}^2_{23}$, the corresponding quantities in the b-quark sector are proportional to $\mathcal{M}^2_{13}$.

and the amount of CP violation. They are given by $M_{H^\pm}$ and its coupling to quarks, (3.22), i.e., on $\tan\beta$. On the other hand, constraints involving the neutral ones depend on the details of the couplings, i.e., they depend sensitively on the rotation matrix R as well as on the neutral Higgs mass spectrum. We shall first review the constraints that depend only on the charged Higgs sector.

In subsections 4.2–4.5 we discuss constraints on the model that depend on the neutral sector. For the purpose of determining these constraints, one has to generalize some predictions for the CP-conserving case to the CP-violating case. Eqs. (4.3), (4.10), (4.12), (4.13) and (4.16) are the results of such generalizations. In the CP-conserving limit, $R_{13} = R_{23} = R_{31} = R_{32} = 0$, and these expressions simplify accordingly.

4.1 Constraints on the charged-Higgs sector

There are three important indirect constraints on the charged-Higgs sector: the B_d^0–$\bar{B}_d^0$ oscillations, R_b and $b \to s\gamma$.

The mass splitting in the neutral B_d mesons is sensitive to contributions from box diagrams with top quark and charged Higgs exchange [34–37], involving the Yukawa couplings (3.22). Indeed, the diagrams with one or two $H^\pm$ exchanges give contributions proportional to $(m_t \cot\beta)^2$ or $(m_t \cot\beta)^4$ multiplied by functions of $M_{H^\pm}$ that for large $M_{H^\pm}$ behave like $1/M_{H^\pm}^2$. These contributions to ΔM_{B_d} will constrain low values of $M_{H^\pm}$, in particular at low values of $\tan\beta$.

While ΔM_{B_d} is known experimentally to considerable precision, $\Delta M_{B_d} = (3.304 \pm 0.046) \times 10^{-10}$ MeV [13], its theoretical understanding is more limited. The largest theoretical uncertainty is related to the parameter combination $f_B^2 B_B$ of the hadronic matrix element. This is only known to a precision of 10–15%. Thus, we cannot exclude models which give predictions for ΔM_{B_d} that deviate from the SM value by this order of magnitude, even if this deviation is large compared to the experimental precision.

In table 1 we show the contribution to ΔM_b^0 that are due to the additional 2HDM fields, for the two parameter sets considered. It is clear that $\tan\beta = 0.5$ is incompatible with the experimental and theoretical constraints on ΔM_b^0, whereas the $\tan\beta = 1.0$ case is marginal.

$\tan\beta$	0.5	1.0	2.0
Set B: $M_{H^\pm} = 300$ GeV	270%	45%	10%
Set A: $M_{H^\pm} = 500$ GeV	140%	24%	5%

Table 1: 2HDM contribution to ΔM_b^0 for parameter sets A and B, relative to its absolute value.

As mentioned above, the $b \to s\gamma$ constraints [14] also force $M_{H^\pm}$ to be high, in particular for low $\tan\beta$. A recent analysis arrived at the bound $M_{H^\pm} \geq 300$ GeV [38]. However, at the very low values of $\tan\beta$ considered here, they are less severe than the ΔM_b^0 and R_b constraints. The experimental constraints on R_b (see sect. 4.5) depend on the charged Higgs mass as well as on the neutral Higgs spectrum. However, this constraint is for low values of $\tan\beta$ practically independent of the neutral spectrum.

4.2 Higgs non-discovery at LEP

One might think that both parameter Set A and Set B would be in conflict with the negative direct searches at LEP, because of the low values of M_1. However, these bounds are marginally evaded by two facts which both dilute the experimental sensitivity. First, the H_1ZZ coupling is suppressed by the square of the Higgs-vector-vector coupling, which relative to the Standard-Model coupling is

$$H_jZZ: \qquad [\cos\beta R_{j1} + \sin\beta R_{j2}], \quad \text{for } j = 1. \tag{4.1}$$

For large values of $|\sin\alpha_1|$ (which is of interest in order to maximise $\gamma_{CP}^{(1)}$ of (3.24)), R_{11} will be rather small, and the second term in (4.1), proportional to R_{12}, takes over. But this is suppressed by the factor $\sin\beta$. For some quantitative studies of this suppression, which can easily be by a factor of 2 or more, see Fig. 8 in [11]. Secondly, the typical decay channel, $H_1 \to b\bar{b}$, is suppressed by the square of the Yukawa coupling, Eq. (3.21). For small values of $\tan\beta$, this is approximately $\cos^2\alpha_1 \cos^2\alpha_2 + \sin^2\beta \sin^2\alpha_2$. In the limits of interest, both terms are small.

In the analysis of LEP data by DELPHI[3], a channel-specific dilution factor C^2 is defined

[3]There are such studies also by the other LEP collaborations (see, for example [17]), but limited to the CP-conserving case.

by [16]

$$\sigma_{Z(h\to X)} = \sigma_{Zh}^{\rm ew} \times C^2_{Z(h\to X)}, \tag{4.2}$$

where $\sigma_{Zh}^{\rm ew}$ is the Standard Model cross section for a particular Higgs mass M. In the 2HDM, for an H_1 decaying to $b\bar{b}$ or $\tau\bar{\tau}$, the dilution is caused by the two effects discussed above: There is a reduced coupling to the Z boson [see (4.1)] and a modified (typically reduced) coupling to the $b\bar{b}$ (or $\tau\bar{\tau}$) [see (3.21)]. Thus, we take

$$C^2_{Z(H_1\to b\bar{b})} = [\cos\beta R_{11} + \sin\beta R_{12}]^2 \, \frac{1}{\cos^2\beta} \, [R_{11}^2 + \sin^2\beta R_{13}^2], \tag{4.3}$$

and consider as excluded parameter sets those where this quantity exceeds the LEP bounds, roughly approximated as [16]

$$C^2_{Z(H_1\to b\bar{b})} = 0.2 \quad \text{at 100 GeV}, \quad \text{and 0.1 at 80 GeV}. \tag{4.4}$$

The last term in (3.21), involving R_{13}, is absent in the CP-conserving case. However, at small $\tan\beta$, it has little effect. Actually, similar results are obtained for both the $b\bar{b}$ and $\tau\bar{\tau}$ channels. Presumably, when these are combined, a more strict limit would be obtained.

It is instructive to consider this expression (4.3) and the corresponding constraints in three simple limits:

$$\tan\beta \ll 1: \qquad C^2_{Z(H_1\to b\bar{b})} \simeq \cos^4\alpha_1 \cos^4\alpha_2 \ll 1. \tag{4.5}$$

This requires either $\alpha_1 \to \pm\pi/2$ or $\alpha_2 \to \pm\pi/2$.

$$\tan\beta = 1: \qquad C^2_{Z(H_1\to b\bar{b})} \simeq [(\cos\alpha_1 + \sin\alpha_1)\cos\alpha_2]^2[\cos^2\alpha_1\cos^2\alpha_2 + \tfrac{1}{2}\sin^2\alpha_2] \ll 1. \tag{4.6}$$

This requires either $\alpha_2 \to \pm\pi/2$ or $\alpha_1 \to -\pi/4$ or $\{\alpha_1 \to \pm\pi/2$ and $\alpha_2 \to 0\}$.

$$\tan\beta \gg 1: \qquad C^2_{Z(H_1\to b\bar{b})} \simeq \tan^2\beta \sin^2\alpha_1 \cos^2\alpha_2[\cos^2\alpha_1\cos^2\alpha_2 + \sin^2\beta\sin^2\alpha_2] \ll 1. \tag{4.7}$$

This requires $\alpha_1 \to 0$ or $\alpha_2 \to \pm\pi/2$ or $\{\alpha_1 \to \pm\pi/2$ and $\alpha_2 \to 0\}$.

Furthermore, we note that at negative α_1, the LEP bound is to some extent evaded for small and medium $|\alpha_2|$ by cancellation among the two terms in the H_1ZZ coupling.

4.3 The ρ-parameter constraint

A very important constraint coming from electroweak precision data, is the precise determination of the ρ-parameter [39, 40]. The quantity

$$\Delta\rho \equiv \frac{1}{M_W^2}\big[A_{WW}(q^2=0) - \cos^2\theta_W A_{ZZ}(q^2=0)\big] \tag{4.8}$$

measures how much the W and Z self-energies can deviate from the Standard-Model value, being zero at the tree level. The experiments (mostly at LEP) have put severe constraints on ρ [41]:

$$\rho = 1.0050 \pm 0.0010. \tag{4.9}$$

The measured deviation from unity is accommodated within the Standard Model, and mostly due to the heavy top quark.

In the 2HDM additional contributions arise [15], which are determined by the couplings to the W and the Z of the Higgs particles, and by the mass splittings within the Higgs sector, as well as the mass splittings with respect to the W and Z bosons. The simplified forms provided in [10] can easily be re-expressed in terms of the mass eigenvalues and the elements R_{jk} of the rotation matrix for the CP-violating basis. For the Higgs–Higgs contribution, we find (the relevant couplings are given in Appendix B):

$$\begin{aligned}
&A_{WW}^{HH}(0) - \cos^2\theta_W\, A_{ZZ}^{HH}(0) \\
&= \frac{g^2}{64\pi^2}\sum_j \Big[\{[\sin\beta R_{j1} - \cos\beta R_{j2}]^2 + R_{j3}^2\} F_{\Delta\rho}(M_{H^\pm}^2, M_j^2) \\
&\quad - \sum_{k>j}[(\sin\beta R_{j1} - \cos\beta R_{j2})R_{k3} - (\sin\beta R_{k1} - \cos\beta R_{k2})R_{j3}]^2\, F_{\Delta\rho}(M_j^2, M_k^2)\Big],
\end{aligned} \tag{4.10}$$

where

$$F_{\Delta\rho}(m_1^2, m_2^2) = \tfrac{1}{2}(m_1^2 + m_2^2) - \frac{m_1^2 m_2^2}{m_1^2 - m_2^2}\log\frac{m_1^2}{m_2^2}. \tag{4.11}$$

For the Higgs–ghost contribution, we have to subtract the contribution from a Standard-Model Higgs of mass M_0, since this is already taken into account in the fits, and find:

$$\begin{aligned}
&A_{WW}^{HG}(0) - \cos^2\theta_W\, A_{ZZ}^{HG}(0) \\
&= \frac{g^2}{64\pi^2}\Big[\sum_j [\cos\beta\, R_{j1} + \sin\beta\, R_{j2}]^2 \Big(3F_{\Delta\rho}(M_Z^2, M_j^2) - 3F_{\Delta\rho}(M_W^2, M_j^2)\Big)
\end{aligned}$$

$$+ 3F_{\Delta\rho}(M_W^2, M_0^2) - 3F_{\Delta\rho}(M_Z^2, M_0^2)\Big]. \tag{4.12}$$

From the electroweak fits, we take $M_0 = 129$ GeV, but note that this value is not very precise [41]. In the CP-conserving limit, these expressions (4.10) and (4.12) simplify considerably, since terms with R_{13}, R_{23}, R_{31}, and R_{32} are absent.

In order to keep these additional contributions (4.10) and (4.12) small, the charged Higgs boson should not be coupled too strongly to the W if its mass is far from those of its neutral partners. As a measure of the "tolerance" we take 3σ, i.e., we impose $|\Delta\rho| \leq 0.003$.

4.4 The muon anomalous magnetic moment

The dominant contribution of the Higgs fields to the muon anomalous magnetic moment, is according to refs. [42] and [25] due to the two-loop Barr–Zee effect [43], with a photon and a Higgs field connected to a heavy fermion loop. The contributions are given by [25] in terms of scalar and pseudoscalar Yukawa couplings. Re-expressed in terms of the Yukawa couplings of (3.21), assuming that the muon couples to the Higgs fields like a down quark, i.e., to Φ_1, we find for the top quark contribution:

$$\Delta a_\mu = \frac{N_c \alpha_{\text{e.m.}}}{4\pi^3 v^2}\, m_\mu^2 Q_t^2 \sum_j \left[R_{j3}^2\, g\left(\frac{m_t^2}{M_j^2}\right) - \frac{1}{\cos\beta \sin\beta}\, R_{j1} R_{j2}\, f\left(\frac{m_t^2}{M_j^2}\right)\right], \tag{4.13}$$

with $N_c = 3$ the number of colours associated with the fermion loop, $\alpha_{\text{e.m.}}$ the electromagnetic finestructure constant, $Q_t = 2/3$ and m_t the top quark charge and mass, and m_μ the muon mass. The functions f and g are given in [43]. It is worth noting that the $\tan\beta$ factor associated with the pseudoscalar Yukawa coupling of the muon is cancelled by an opposite factor associated with the top quark. While the first term gives a positive contribution, the second one may have either sign.

The contribution of the b quark can be obtained from (4.13) by trivial substitutions for Q_t and m_t accompanied by

$$R_{j3}^2 \to \tan^2\beta R_{j3}^2, \quad \text{and} \quad \frac{1}{\cos\beta\sin\beta} R_{j1} R_{j2} \to \frac{1}{\cos^2\beta} R_{j1}^2 \tag{4.14}$$

in the square bracket.

Earlier studies (see, for example, [25,42]) have focused on the contributions from rather light pseudoscalars and large $\tan\beta$, where the b and τ contributions are enhanced by the

substitutions (4.14). At high $\tan\beta$, the b-quark loop will indeed dominate. For small values of $\tan\beta$, as are considered here, the b-quark contribution is completely negligible.

The experimental situation is somewhat unclear, depending on how the hadronic corrections to the running of $\alpha_{\rm e.m.}$ are evaluated. The deviation from the Standard Model can be summarized as [44]

$$\Delta a_\mu^{\rm exp} - \Delta a_\mu^{\rm SM} = \begin{cases} (221-245)\times 10^{-11}, & e^+e^-, \\ (62-142)\times 10^{-11}, & \tau^+\tau^-, \{e^+e^- \;\&\; \tau^+\tau^-\}, \end{cases} \tag{4.15}$$

and represent 0.7 to 2.8 standard deviations with respect to the data [45]. Two distinct attitudes are here possible. One may either fit this (positive) deviation with some new physics effect [25], or one may restrict new physics contributions not to exceed this contribution (4.15). We shall here follow this latter approach, and require the 2HDM contribution (4.13) to be less than 3σ, i.e., $|\Delta a_\mu| < 300\times 10^{-11}$. For the parameters considered here, $\tan\beta \le \mathcal{O}(2)$, the 2HDM contribution to Δa_μ is at most (a few) $\times\, 10^{-11}$ and therefore plays no role in constraining the model.

4.5 R_b

The one-loop contributions to the $Zb\bar{b}$ coupling influence the relative branching ratio of $Z\to b\bar{b}$, given by R_b, which is known to 0.05%, or 1.25 MeV precision [13]. In the SM there are significant contributions proportional to m_t^2. In the 2HDM there are additional one-loop contributions due to triangle diagrams involving charged and (non-standard) neutral-Higgs fields. For the CP-conserving case, these were given in [46]. In the general CP-violating case, the charged-Higgs contribution, Eq. (4.2) of [46], remains unchanged, but we find that the neutral-Higgs part, Eq. (4.4), gets modified to

$$\begin{aligned}\delta\Gamma_V^f(H) = \frac{\alpha_{\rm e.m}^2 N_c\, m_Z}{96\pi \sin^4\theta_W \cos^2\theta_W}\,\frac{m_b^2}{m_W^2}\Bigg\{\sum_{j=1}^{3}\Bigg[\sum_{k=1}^{3}[(\sin\beta R_{j1}-\cos\beta R_{j2})R_{k3} \\ -(\sin\beta R_{k1}-\cos\beta R_{k2})R_{j3}]\frac{\tan\beta}{\cos\beta}\,R_{j1}R_{k3}\,\rho_4(m_Z^2,M_j^2,M_k^2,0) \\ -(\cos\beta R_{j1}+\sin\beta R_{j2})\frac{R_{j1}}{\cos\beta}\,\rho_4(m_Z^2,M_j^2,m_Z^2,0) \\ +2Q_b\sin^2\theta_W(1+2Q_b\sin^2\theta_W)\left(\frac{R_{j1}^2}{\cos^2\beta}+\tan^2\beta R_{j3}^2\right)\rho_3(m_Z^2,M_j^2,0)\Bigg]\end{aligned}$$

$$+ 2Q_b \sin^2\theta_W (1 + 2Q_b \sin^2\theta_W)\, \rho_3(m_Z^2, m_Z^2, 0) \Big\}. \tag{4.16}$$

The functions ρ_3 and ρ_4 are various combinations of three-point and two-point loop integrals [46]. For the numerical studies, we use the `LoopTools` package [47, 48]. Again, this expression (4.16) is more complicated than those of the CP-conserving limit, but the additional terms have little quantitative importance at low $\tan\beta$.

$\tan\beta$	0.5	1.0	2.0
Set B: $M_{H^\pm} = 300$ GeV	5.6	1.4	0.35
Set A: $M_{H^\pm} = 500$ GeV	3.3	0.83	0.21

Table 2: 2HDM contribution to R_b for parameter sets A and B, in units of the uncertainty, $\sigma(R_b) = 1.25$ MeV.

At small $\tan\beta$, the charged-Higgs contribution, which behaves like $(m_t/\tan\beta)^2$ due to the $H^+ b\bar{t}$ and $H^- \bar{b} t$ couplings, dominates. For $M_{H^\pm} = 500$ GeV (Set A) and $M_{H^\pm} = 300$ GeV (Set B) the 2HDM contributions to R_b are given in Table 2. For the two larger values of $\tan\beta$, this is compatible with the experimental uncertainty, whereas for $\tan\beta = 0.5$ it amounts to a substantial conflict, especially for the lower value of $M_{H^\pm}$ (Set B). The neutral-Higgs contribution, as given by (4.16), is smaller, by three orders of magnitude.

5 Overview over allowed parameters

5.1 Variations of mass parameters around Set A

We start this discussion of model parameters by a survey of how the allowed regions of the α_2–α_3 space depend on the mass parameters, in particular M_3, $M_{H^\pm}$ and μ^2. It turns out that while stability is readily satisfied for "relevant" mass parameters, unitarity excludes sizable regions of parameter space. Ignoring experimental constraints, a low-mass spectrum is in general easier to accommodate than one where some Higgs particles are heavy. In many cases, non-zero values of λ_6 and λ_7 also have a tendency to reduce the allowed parameter space.

In Fig. 1 we show for Set A the allowed regions in the α_2–α_3 plane, for a few representative values of α_1, focusing on stability (or positivity) and unitarity. For the considered

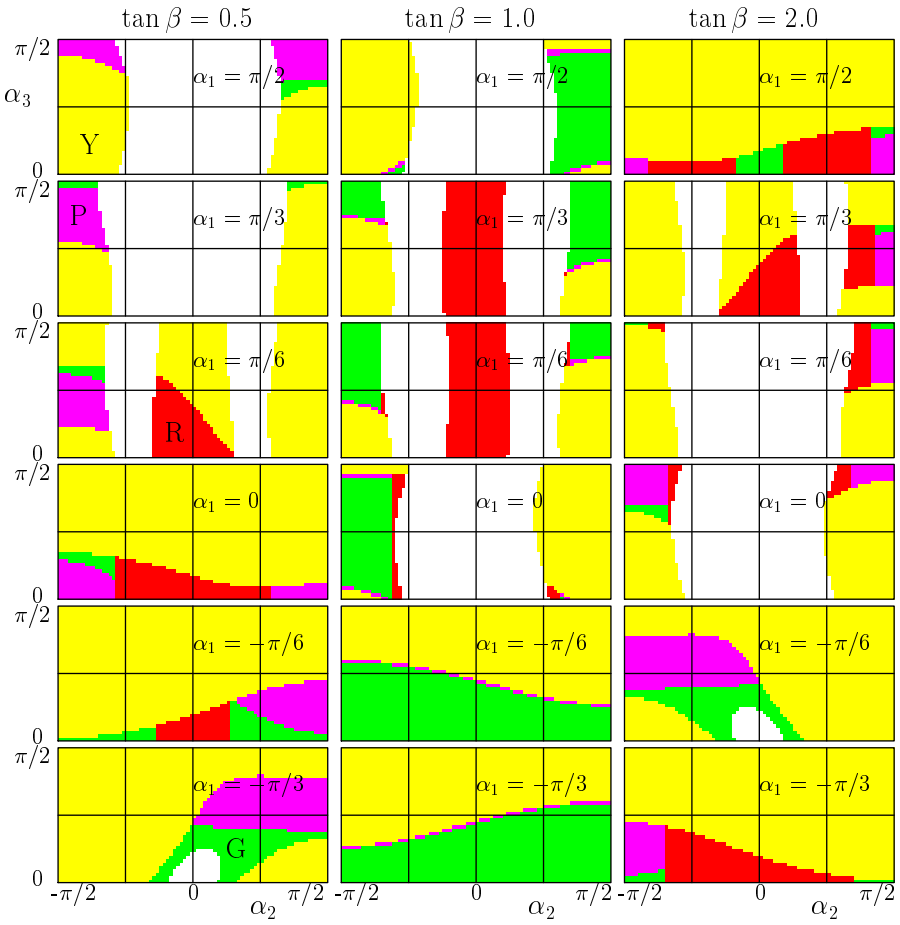

Figure 1: Allowed and forbidden regions in the α_2–α_3 plane, for $\tan\beta = 0.5$, 1 and 2, parameter Set A and selected values of α_1. Green (G): stability, unitarity, direct search and $\Delta\rho$ constraints satisfied; red (R) [purple (P)]: stability, unitarity satisfied, but direct search [and $\Delta\rho$] constraints not satisfied; yellow (Y): stability (but not unitarity) satisfied; white: stability violated.

parameters, much of the α_2–α_3 plane is actually in violation of stability, as shown in white. Next, there are significant areas (yellow) where stability is satisfied, but (tree-level) unitarity is violated. Finally, in darker colours, we indicate where also unitarity holds. Part of these areas (typically, small $|\alpha_2|$, as discussed in sect. 4.2) are in conflict with the direct search (LEP) data, and indicated in red. Some areas (purple, typically, larger $|\alpha_2|$) violate the $\Delta\rho$ constraint, whereas the remaining areas in green give viable models. The symmetry given by Eq. (3.11) is evident in the figure: the case of $\tan\beta = 2$ can be obtained from the case of $\tan\beta = 0.5$ by suitable reflections, apart from the experimental constraints, which

in the 2HDM (II) distinguish $\tan\beta$ and $\cot\beta$. For $\tan\beta > 1$, the direct search constraints shift from those of (4.5) towards those of (4.7).

While this figure can not be directly compared with Fig. 7 of ref. [11], since we here keep M_3 fixed, it was found that the unitarity constraints of [30, 32] are more restrictive than the order-of-magnitude estimate adopted in [11]. It should also be noted that with $\mathrm{Im}\,\lambda_5 = 0$, as given by the parameter Set A, $\mathrm{Im}\,\lambda_6$ and $\mathrm{Im}\,\lambda_7$ will be non-zero in the general CP-violating case.

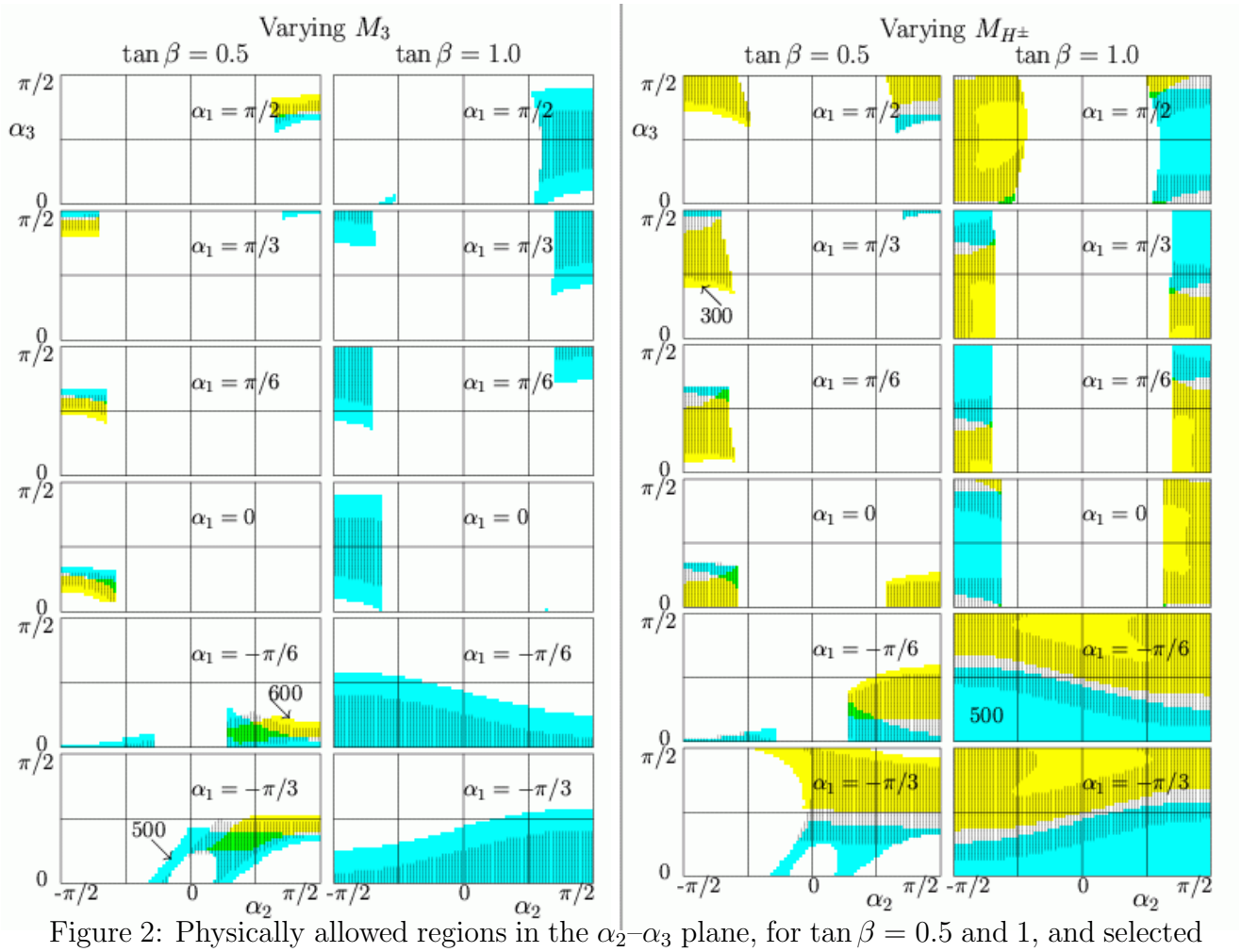

Figure 2: Physically allowed regions in the α_2–α_3 plane, for $\tan\beta = 0.5$ and 1, and selected values of α_1. Left: Variations of M_3 around parameter Set A. Blue: $M_3 = 500$ GeV (Set A), vertical lines: $M_3 = 550$ GeV, yellow: $M_3 = 600$ GeV. Note that some regions overlap. In particular, green denotes regions allowed for both $M_3 = 500$ GeV and $M_3 = 600$ GeV. Right: Variations of $M_{H^\pm}$ around parameter Set A. Yellow: $M_{H^\pm} = 300$ GeV, vertical lines: $M_{H^\pm} = 400$ GeV, blue: $M_{H^\pm} = 500$ GeV (Set A).

Dependence on M_3 and M_2. The dependence of the allowed regions on M_3, the heaviest neutral Higgs boson, is illustrated in Fig. 2 (left), for the other parameters kept fixed at the values of parameter Set A. The figure shows the allowed regions for $M_3 = 500$ GeV (blue, default of Fig. 1), 550 GeV (vertical lines) and 600 GeV (yellow). Smaller allowed regions are also found at 450 and 650 GeV (not shown), but nothing neither at 400 GeV nor at 700 GeV.

As M_2 approaches M_1, there are still regions where stability is satisfied, but unitarity is only satisfied in very small regions. Similarly, as discussed above, when M_2 approaches M_3, the allowed regions tend to be restricted to small values of $|\alpha_2| \to 0$. Thus, by (3.34), there is in this limit of $M_1 \ll M_2 \lesssim M_3$, little CP violation in the top-quark sector.

Dependence on $M_H^\pm$. The dependence of the allowed regions on $M_{H^\pm}$, the charged Higgs boson, is illustrated in Fig. 2 (right), for the other parameters kept fixed at the values of parameter Set A. The allowed region is seen to increase a bit for lower values of $M_{H^\pm}$, but such values are constrained by the ΔM_{B_d}, R_b [13] and $b \to s\gamma$ data [14], especially at low values of $\tan\beta$. On the other hand, the allowed regions shrink for high values of $M_{H^\pm}$. Nothing is allowed at $M_H^\pm \geq 600$ GeV. The shrinking of the allowed regions for high values of $M_{H^\pm}$ is due to the $\Delta\rho$ constraint at large $|\alpha_2|$ and/or negative α_1, as well as the direct search (LEP) constraint at small $|\alpha_2|$. Eventually (like for high values of M_3) also the unitarity constraint excludes high values of $M_H^\pm$.

Dependence on μ^2. Since $\lambda_4 + \mathrm{Re}\,\lambda_5$ is bounded from below by the stability requirement [see (A.23)], the parameter μ^2 normally plays a role in pushing $M_{H^\pm}$ to values that are high enough to evade the R_b, ΔM_{B_d} [13] and $b \to s\gamma$ constraints. In Fig. 3 we show how the allowed region in the α_2–α_3 plane shrinks for "low" and "high" values of μ^2, when the Higgs boson masses and other parameters are kept fixed. For the considered spectrum of masses, a range of negative values of μ^2 is allowed (for $\mu^2 = -(400\ \mathrm{GeV})^2$ there are no allowed regions). For increasing positive values of μ^2, the allowed regions shrink away before $\mu^2 = (400\ \mathrm{GeV})^2$ (which is not allowed). Of course, these critical values depend on the mass spectrum adopted in parameter Set A.

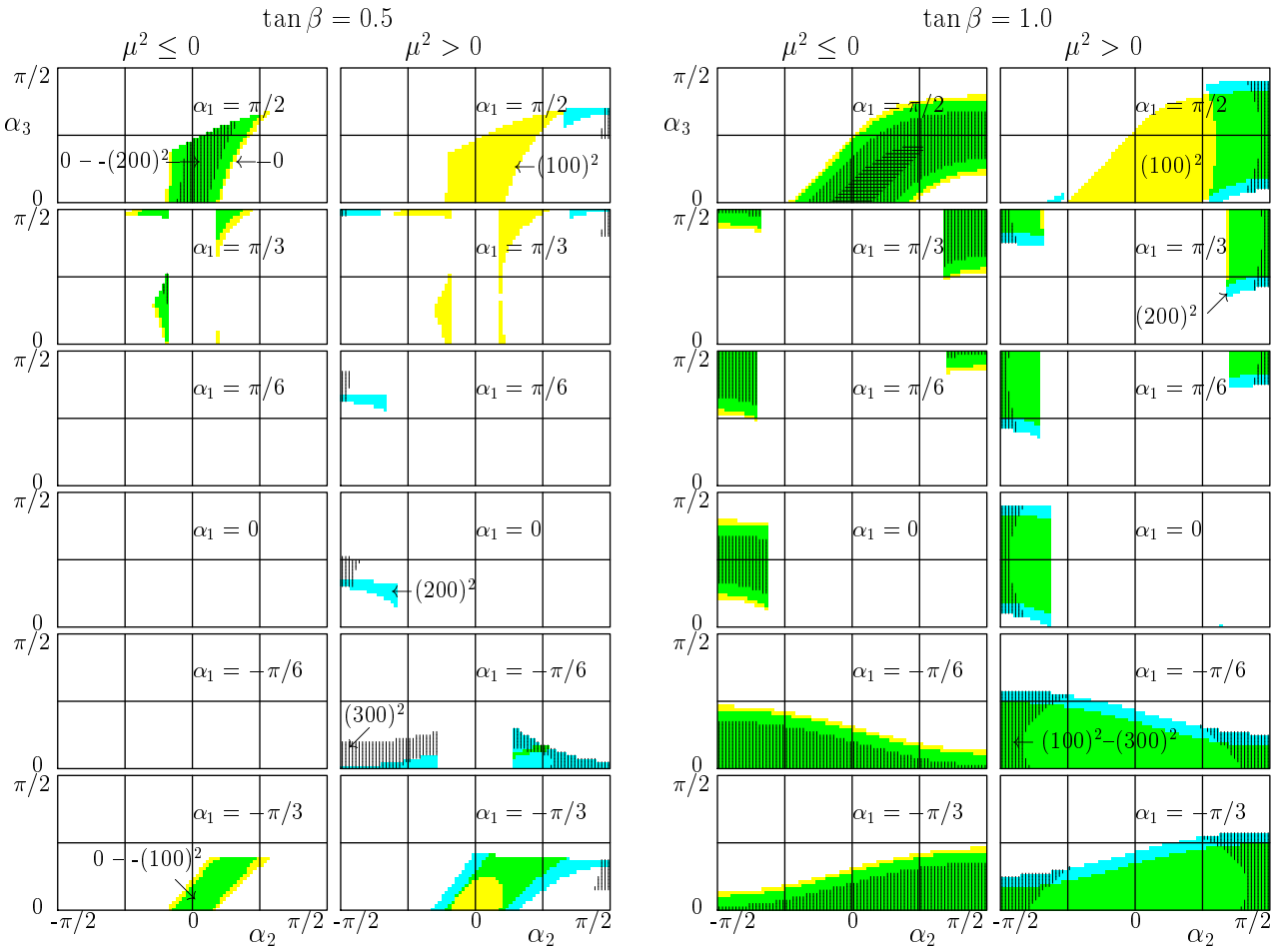

Figure 3: Physically allowed regions in the α_2–α_3 plane, for $\tan\beta = 0.5$ and 1, and selected values of α_1. Variations around parameter Set A; $\mu^2 \leq 0$ and $\mu^2 > 0$ shown separately. $\mu^2 \leq 0$: Yellow: $\mu^2 = 0$, green: $\mu^2 = -(100\text{ GeV})^2$, vertical lines: $\mu^2 = -(200\text{ GeV})^2$. $\mu^2 > 0$: Yellow: $\mu^2 = (100\text{ GeV})^2$, blue: $\mu^2 = (200\text{ GeV})^2$, vertical lines: $\mu^2 = (300\text{ GeV})^2$. Note that some regions overlap. In particular, for $\mu^2 > 0$, green is allowed for both $\mu^2 = (100\text{ GeV})^2$ and $\mu^2 = (200\text{ GeV})^2$.

5.2 Variations of mass parameters around Set B

We shall here briefly review the light-Higgs scenario of parameter Set B, but recall that the $\tan\beta = 0.5$ case is essentially ruled out by the ΔM_b^0 data.

In Fig. 4 we show for $\mu^2 = 0$ how stability can be satisfied in the *whole* α_2–α_3 plane. For $\tan\beta = 1$, stability and unitarity would actually allow any value of the rotation matrix R, i.e., any values of α_1, α_2 and α_3. However, except for this special case, unitarity is only satisfied in parts of the plane.

The direct search (LEP) constraint severely cuts into the allowed regions of this light-

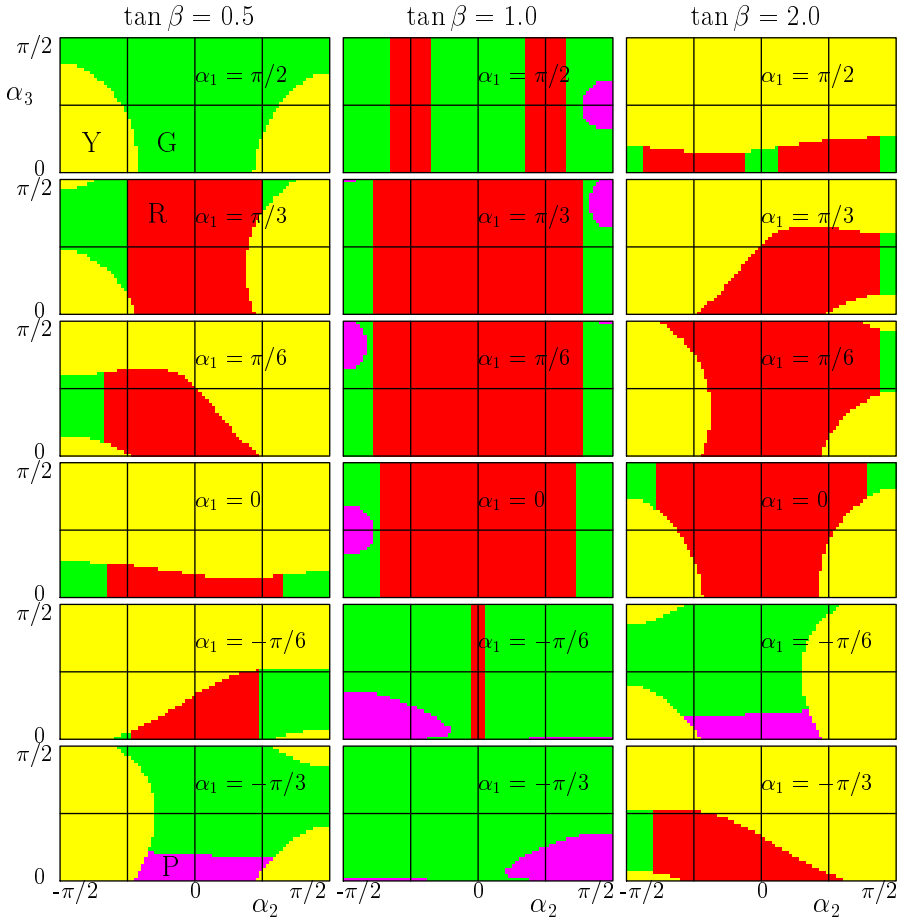

Figure 4: Stability and unitarity in the α_2–α_3 plane, for $\tan\beta = 0.5$, 1 and 2, parameter Set B with $M_3 = 400$ GeV, $\mu^2 = 0$ and selected values of α_1. Colour codes as in Fig. 1.

Higgs (set B) scenario, with $C^2 = 0.1$ [16], see sect. 4.2. As noted there, this constraint tends to exclude the central range of small $|\alpha_2|$ and positive and small α_1.

Increasing μ^2 to $(200\ \text{GeV})^2$, the most striking change is perhaps the emergence of large regions where stability is not satisfied (indicated in white in Fig. 5). Another interesting observation is that for $\tan\beta = 1.0$ and negative values of α_1, the picture is little changed from the case of $\mu^2 = 0$.

With a higher value of M_3 ($M_3 = 600$ GeV, but $\mu^2 = 0$), the unitarity constraint excludes most of the α_2–α_3 plane. For $\tan\beta = 1.0$ the whole plane is excluded.

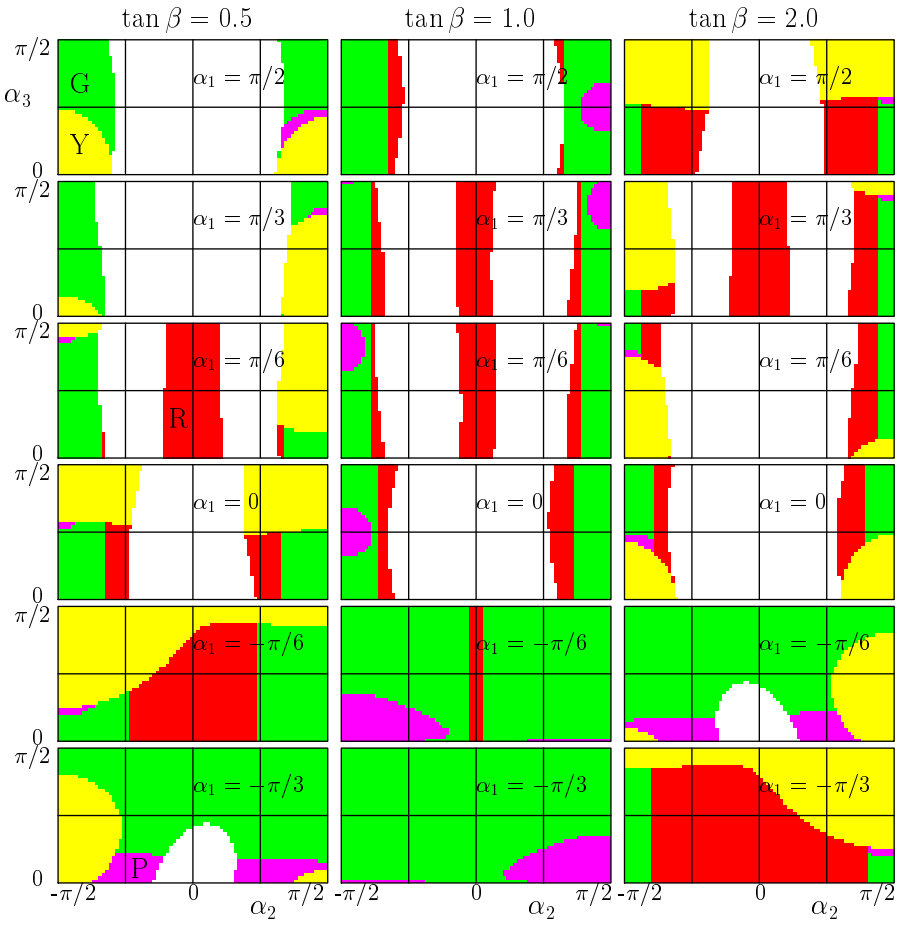

Figure 5: Stability and unitarity in the α_2–α_3 plane, for $\tan\beta = 0.5$, 1 and 2, parameter Set B with $M_3 = 400$ GeV, $\mu^2 = (200\text{ GeV})^2$ and selected values of α_1. Colour codes as in Fig. 1.

5.3 Non-zero values of $\mathrm{Im}\,\lambda_5$, $\mathrm{Re}\,\lambda_6$, $\mathrm{Re}\,\lambda_7$

This subsection will present a brief discussion of how the allowed regions get modified for non-zero values of parameters which are normally set to zero, in order to control the amount of Flavour-Changing Neutral Currents. Thus, adopting a non-zero value for any of them in a "realistic" model would have to be done with an eye to these effects.

5.3.1 Non-zero values of $\mathrm{Im}\,\lambda_5$

The cases of positive and negative values of $\mathrm{Im}\,\lambda_5$ can be related. This is seen as follows: by the transformation C3 of (3.6) and (3.8), the mass-squared elements $\mathcal{M}^2_{13}$ and $\mathcal{M}^2_{23}$ flip signs, and the auxiliary quantities $\mathrm{Im}\,\lambda_6$ and $\mathrm{Im}\,\lambda_7$ change signs without altering the

stability or unitarity constraints. The only effect will be that CP-violating effects change sign. Thus, we may restrict the discussion of non-zero $\mathrm{Im}\,\lambda_5$ to $\mathrm{Im}\,\lambda_5 > 0$. However, the full range (3.7) of α_3 now has to be considered.

We show in Fig. 6, for some values of $\tan\beta$ and α_1, and for parameter Set A how non-zero values of $\mathrm{Im}\,\lambda_5$ also provide allowed regions in the α_2–α_3 plane. But these are typically smaller for higher values of $\mathrm{Im}\,\lambda_5$, and rather scattered. However, they can lead to significant CP violation, since allowed ranges of $|\alpha_2|$ tend to be at intermediate values of $|\alpha_2|$ [see Eq. (3.17)].

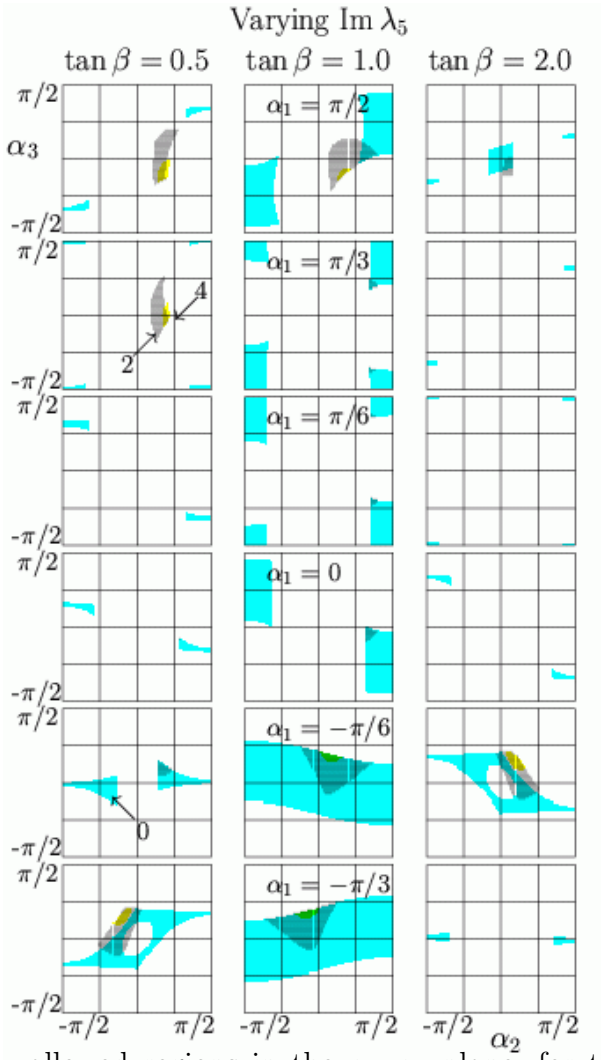

Figure 6: Physically allowed regions in the α_2–α_3 plane, for $\tan\beta = 0.5$, 1 and 2, and selected values of α_1. Variations of $\mathrm{Im}\,\lambda_5$ around parameter Set A. Blue: $\mathrm{Im}\,\lambda_5 = 0$, vertical lines: $\mathrm{Im}\,\lambda_5 = 2$, yellow: $\mathrm{Im}\,\lambda_5 = 4$.

5.3.2 Non-zero values of $\mathrm{Re}\,\lambda_6$ or $\mathrm{Re}\,\lambda_7$

Up to this point, we have kept $\mathrm{Re}\,\lambda_6 = \mathrm{Re}\,\lambda_7 = 0$. However, we have treated $\mathrm{Im}\,\lambda_6$ and $\mathrm{Im}\,\lambda_7$ as auxiliary quantities derived from the spectrum, the rotation matrix and $\mathrm{Im}\,\lambda_5$ via Eq. (3.3). In general, they will be non-zero. This might lead to too large flavour-changing neutral couplings, due to the violation of the Z_2 symmetry [2, 27, 28]. We have not investigated this constraint quantitatively, but note that in many cases the imaginary parts of λ_6 and λ_7 can be shifted to the imaginary part of λ_5 [see (2.10)]. This will however lead to a modification of the rotation matrix R and/or the spectrum, by for example a shift in M_3 according to the approach of [11].

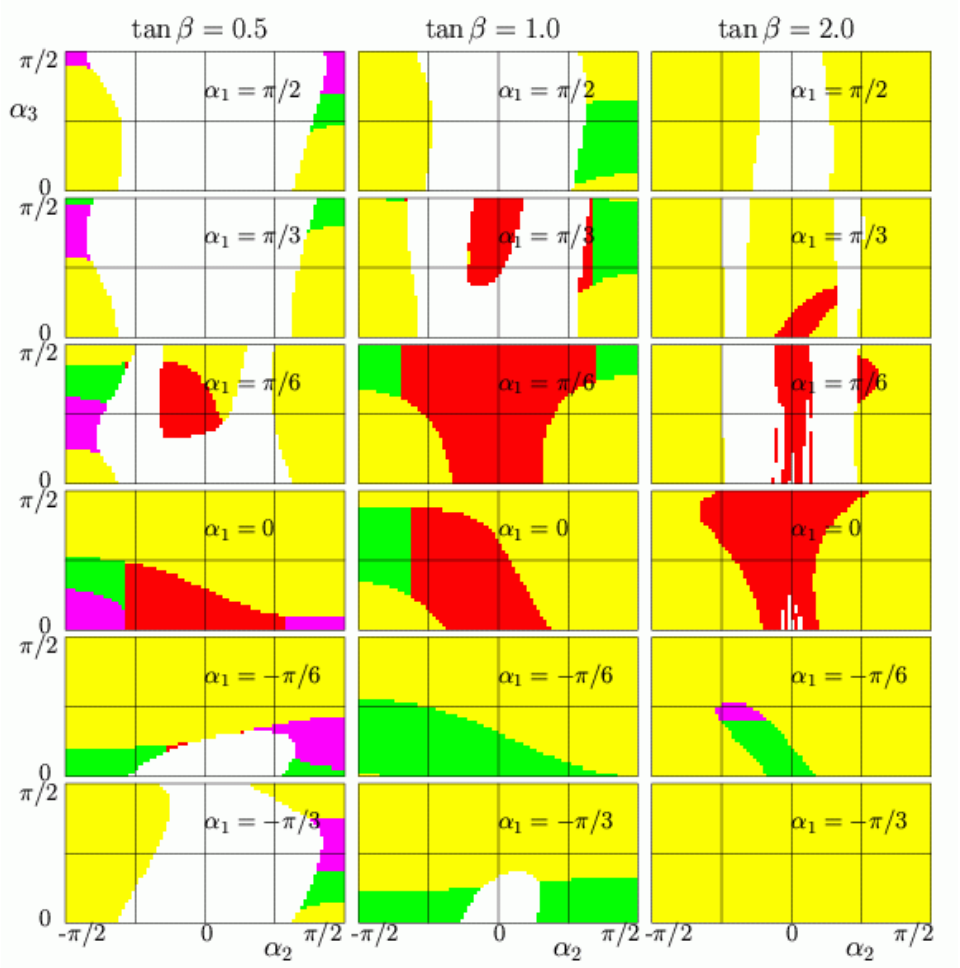

Figure 7: Physically allowed regions in the α_2–α_3 plane, for $\tan\beta = 0.5$, 1 and 2, and selected values of α_1. Parameters correspond to Set A, except that $\mathrm{Re}\,\lambda_6 = -1$. Colour codes as in Fig. 1.

The Yukawa interactions (see sect. 3.5) couple the Higgs fields to a left-handed doublet and a right-handed singlet quark field. However, these need not be in the flavour basis in which the mass matrices are diagonal. The Z_2 symmetry, which is imposed to stabilize Model II [2, 28] is broken by the m_{12}^2 and $\mathrm{Im}\,\lambda_5$ terms, as well as by the λ_6 and λ_7 terms. However, one may adopt the attitude that these terms, which arise naturally in the MSSM [18–22] are constrained and subdominant. Additionally, one may argue that the FCNC's are suppressed by powers of the quark masses [49, 50], thus evading the experimental constraints involving the first two fermion generations.

We shall here only discuss the case of *either* $\mathrm{Re}\,\lambda_6$ *or* $\mathrm{Re}\,\lambda_7$ being non-zero, the other being zero. Because of the symmetry (3.11), (3.12), we may restrict this discussion to $\mathrm{Re}\,\lambda_6 \neq 0$, $\mathrm{Re}\,\lambda_7 = 0$. Analogous results for $\mathrm{Re}\,\lambda_6 = 0$, $\mathrm{Re}\,\lambda_7 \neq 0$ can be obtained from these by the inversion $\tan\beta \leftrightarrow 1/\tan\beta$ according to (3.11) and (3.12).

Even though $\mathrm{Re}\,\lambda_6$ (or $\mathrm{Re}\,\lambda_7$) significantly different from zero may turn out to be ruled out by the constraints on FCNC's, we find it instructive to see how the otherwise allowed regions change when these parameters are introduced.

In Fig. 7 we show the "allowed" regions corresponding to parameter Set A, except that $\mathrm{Re}\,\lambda_6 = -1$. The allowed regions are qualitatively rather similar to those of Fig. 1. However, with $\mathrm{Re}\,\lambda_6 = +1$, stability tends to be violated in most of the α_2–α_3 plane. Also, when $\mathrm{Re}\,\lambda_6$ decreases to -2 or -3, there is nothing allowed at $\tan\beta = 1$ and $\tan\beta = 0.5$, respectively.

6 CP violation in $t\bar{t}$ production at the LHC

In order to illustrate the CP-violating effects that can be observed at the LHC, resulting from mixing in the Higgs sector, we consider the process

$$pp \to t\bar{t} + X, \tag{6.1}$$

which at high energies is dominated by the underlying process

$$gg \to t\bar{t}. \tag{6.2}$$

In the presence of CP violation, correlations will then be induced at the parton level involving the t and $\bar{t}$ spins, denoted $\boldsymbol{s}_1$ and $\boldsymbol{s}_2$, and their c.m. momentum $\boldsymbol{p}$ [8]:

$$\langle \hat{\boldsymbol{p}} \cdot (\boldsymbol{s}_1 - \boldsymbol{s}_2) \rangle, \quad \text{and} \quad \langle \hat{\boldsymbol{p}} \cdot (\boldsymbol{s}_1 \times \boldsymbol{s}_2) \rangle. \tag{6.3}$$

These correlations are determined by the CP-violating combination (3.23) of Yukawa couplings, multiplied by certain loop integrals, and convoluted over the gluon–gluon c.m. energy [8, 11].

The t and $\bar{t}$ quarks decay fast enough that hadronization effects do not smear out these CP-odd correlations. They can thus be treated perturbatively. Consider the semileptonic decays:

$$t \to l^+ \nu_l b, \quad \bar{t} \to l^- \bar{\nu}_l \bar{b}, \tag{6.4}$$

with $l = e^-$ or μ^-. The lepton energies will inherit an asymmetry from the first correlation given in Eq. (6.3), accessible via the observable:

$$A_1 = E_+ - E_-. \tag{6.5}$$

An important question is whether or not this can be large enough to be measurable.

In order to have a significant observation, the expectation value $\langle A_1 \rangle$ must compare favourably with the statistical fluctuations, which behave like $\sqrt{N}$, where N is the number of events. In order to assess this, it is convenient to consider the "signal to noise" ratio [8],

$$\frac{S}{N} = \frac{\langle A_1 \rangle}{\sqrt{\langle A_1^2 \rangle - \langle A_1 \rangle^2}}, \tag{6.6}$$

where the denominator gives the statistical width of the observable (6.5).

Other limitations of this approach include the need for very good lepton energy calibration, and the assumption of no (anomalous) right-handed couplings in the tbW coupling (see [51]).

We display the ratio S/N in Fig. 8, as a function of the mass of the lightest Higgs boson, M_1, for two rotation matrices R, given by the angles $\{\alpha_1, \alpha_2, \alpha_3\}$, and for two values of $\tan\beta$. These parameters are chosen such that the model is consistent (stability and unitarity) and satisfies the experimental constraints (see the discussion in Sect. 5.1 and Fig. 1). The actual evaluation of this quantity (6.6) follows the approach of [11], using

the LoopTools package for the loop evaluations [47, 48] and the CTEQ6 parton distribution functions [52] to describe the gluon content of the proton.

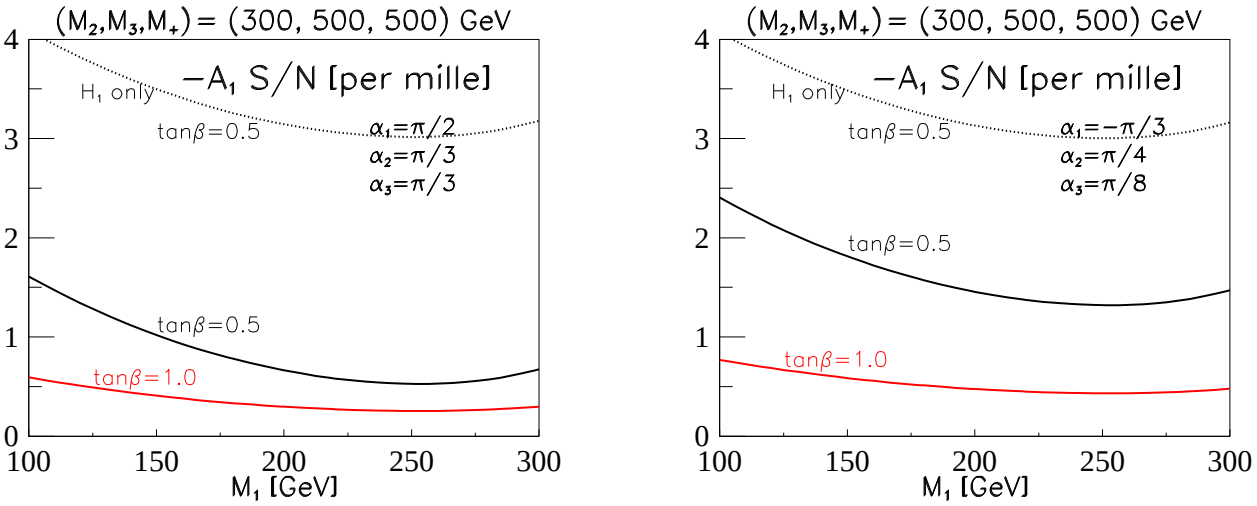

Figure 8: Signal to noise ratio vs. M_1, otherwise parameter Set A. Rotation matrix R defined by angles $\{\alpha_1, \alpha_2, \alpha_3\}$ as indicated. Actually, in the left panel, we show S/N for $-A_1$. Dotted curves: contribution of the lightest Higgs boson only.

While the allowed regions, for $\tan\beta = 0.5$, in Fig. 1 only are rather small and scattered, they remain allowed as M_1 is increased towards M_2. For these two rotation matrices, the contribution of the lightest Higgs boson, H_1, is actually the same (apart from the over-all sign), as shown by the dotted curves. In terms of the quantities (3.23), $|\gamma_{CP}^{(1)}| = 1.936$ is the same for both cases. However, for the case shown on the left, the contribution of H_2 (with $M_2 = 300$ GeV), is with $\gamma_{CP}^{(2)}/\gamma_{CP}^{(1)} = -0.75$ more efficient in reducing the effect of H_1 than for the case on the right, where the corresponding ratio is -0.44.

In general, the values fall with increasing M_1, since the loop integrals decrease. However, there is a resonance in one diagram at $M_j = 2m_t \sim 350$ GeV (for more details, see [11]), this is the reason for the increase beyond 250 GeV.

In Fig. 9 we show, for the same rotation matrices as in Fig. 8, how S/N varies with M_2. Here, some of the curves are cut off at low or high values of M_2, since the model becomes inconsistent or experimentally excluded, as discussed in Sect. 5.1. In some cases, an enhanced negative interference occurs as $M_2 \simeq 2m_t$.

In this study, the parameter μ^2 was allowed to float, as compared with parameter Set A,

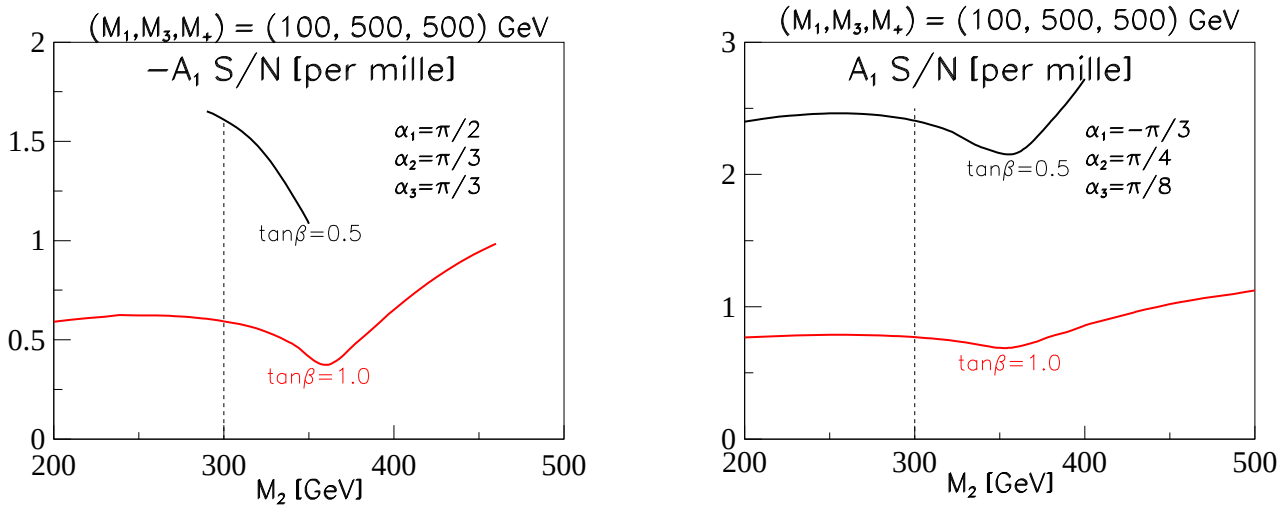

Figure 9: Signal to noise ratio vs. M_2, otherwise parameter Set A. Rotation matrices R as in Fig. 8. Dashed line: value of M_2 in parameter Set A.

in order to extend the range of allowed values of M_2. In all cases, except the right panel, with $\tan\beta = 1$, the value of μ^2 had to be adjusted as follows: At low values of M_2, a lower value of μ^2 was needed, and at high values of M_2, a higher value was needed.

Finally, in Fig. 10, we show the variation of S/N with M_3, keeping M_1 and M_2 fixed. There is a tendency for the value to increase with M_3 (because of reduced destructive interference), but variations of M_3 are only allowed within a rather restricted range (see again Sect. 5.1 and Fig. 2).

7 Summary and conclusions

The constraints of stability and tree-level unitarity exclude most of the multidimensional 2HDM (II) parameter space. Furthermore, the direct searches (LEP) [16] and the $\Delta\rho$ [13] constraints exclude certains domains of the parameters. Finally, the direct searches, as well as the ΔM_{B_d}, R_b [13] and $b \to s\gamma$ [14] constraints exclude a light charged Higgs boson, in particular at low values of $\tan\beta$. The remaining pockets of allowed parameters will for low values of $\tan\beta$ allow CP violation in the top-quark sector, due to the exchange of Higgs bosons that are mixed with respect to CP.

In order to maximize the CP violation in the top-quark sector that might be measurable

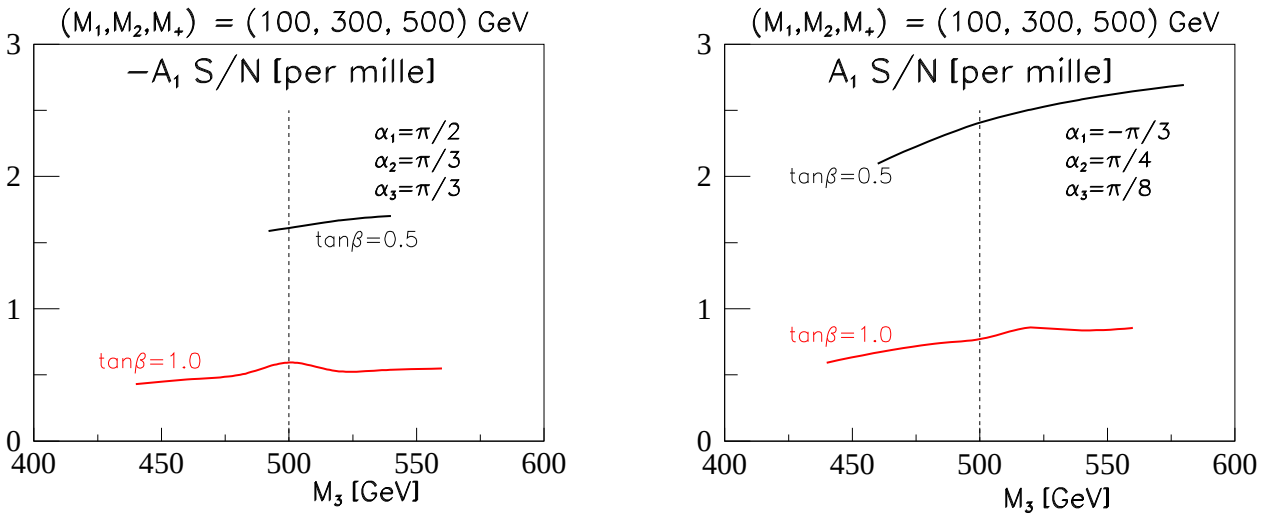

Figure 10: Signal to noise ratio vs. M_3, otherwise parameter Set A. Rotation angles $\{\alpha_1, \alpha_2, \alpha_3\}$ as indicated. Dashed line: value of M_3 in parameter Set A.

at the LHC, we focus on parameters where (i) the lightest Higgs boson is rather light, in order to maximize the relevant loop integrals, and (ii) where the product of the CP-violating Yukawa couplings, parametrized by $\gamma_{CP}^{(1)}$ [see Eq. (3.23)] are large. The latter constraint requires $\tan\beta$ to be small, and $|\sin\alpha_1 \sin 2\alpha_2|$ to be large.

In summary, we note that even in the face of a variety of experimental constraints, the model is consistent in a number of regions in parameter space. Apart from exceptional points, these allowed regions yield CP violation in $t\bar{t}$ final states produced at the LHC, at a level which can be explored with a data sample of the order of 10^6 semileptonic events.

Acknowledgments. It is a pleasure to thank Okan Camursoy and Levent Selbuz for their contributions in the early stages of this work. This research has been supported in part by the Mission Department of Egypt and the Research Council of Norway.

Appendix A

In this Appendix we describe the method used for formulating the necessary and sufficient conditions for the potential to satisfy stability. For earlier approaches to stability, all restricted to simpler potentials, see [53–56]. We start by rewriting the Higgs doublets as:

$$\Phi_1 = ||\Phi_1||\hat{\Phi}_1, \qquad \Phi_2 = ||\Phi_2||\hat{\Phi}_2 \tag{A.1}$$

where $||\Phi_i||$ is the norm of the spinor Φ_i, and $\hat{\Phi}_i$ is a unit spinor. By $SU(2)$ invariance, only four combinations of fields may appear:

$$\Phi_1^\dagger\Phi_1 = ||\Phi_1||^2, \quad \Phi_2^\dagger\Phi_2 = ||\Phi_2||^2, \quad \Phi_2^\dagger\Phi_1 = ||\Phi_1|| \cdot ||\Phi_2|| \left(\hat{\Phi}_2^\dagger \cdot \hat{\Phi}_1\right), \quad \Phi_1^\dagger\Phi_2 = [\Phi_2^\dagger\Phi_1]^*$$

We let the norms $||\Phi_i||$ of eq. (A.1) be parametrized as follows:

$$||\Phi_1|| = r\cos\gamma, \qquad ||\Phi_2|| = r\sin\gamma. \tag{A.2}$$

The complex product $\hat{\Phi}_2^\dagger \cdot \hat{\Phi}_1$ between the two unit spinors will be a complex number $x+iy$ with $|x+iy| \leq 1$.

Using this parametrization, we can write:

$$\begin{aligned} &\Phi_1^\dagger\Phi_1 = r^2\cos^2\gamma, \quad \Phi_2^\dagger\Phi_2 = r^2\sin^2\gamma, \\ &\Phi_2^\dagger\Phi_1 = r^2\cos\gamma\sin\gamma(x+iy), \quad \Phi_1^\dagger\Phi_2 = r^2\cos\gamma\sin\gamma(x-iy), \end{aligned} \tag{A.3}$$

where $r \geq 0$, $\gamma \in [0, \pi/2]$ and $x^2+y^2 \leq 1$.

The potential can now be written as

$$V = r^4 V_4 + r^2 V_2, \tag{A.4}$$

with the quartic part:

$$\begin{aligned} V_4 \;=\; & \lambda_1 A_1 + \lambda_2 A_2 + \lambda_3 A_3 + \lambda_4 A_4 + \mathrm{Re}\,\lambda_5 A_5 + \mathrm{Im}\,\lambda_5 A_6 \\ & + \mathrm{Re}\,\lambda_6 A_7 + \mathrm{Im}\,\lambda_6 A_8 + \mathrm{Re}\,\lambda_7 A_9 + \mathrm{Im}\,\lambda_7 A_{10} \end{aligned} \tag{A.5}$$

where

$$\begin{aligned} &A_1 = \frac{1}{2}\cos^4\gamma, \quad A_2 = \frac{1}{2}\sin^4\gamma, \quad A_3 = \cos^2\gamma\sin^2\gamma, \\ &A_4 = (x^2+y^2)\cos^2\gamma\sin^2\gamma, \quad A_5 = (x^2-y^2)\cos^2\gamma\sin^2\gamma, \quad A_6 = 2xy\cos^2\gamma\sin^2\gamma, \\ &A_7 = 2x\cos^3\gamma\sin\gamma, \quad A_8 = 2y\cos^3\gamma\sin\gamma, \\ &A_9 = 2x\cos\gamma\sin^3\gamma, \quad A_{10} = 2y\cos\gamma\sin^3\gamma. \end{aligned} \tag{A.6}$$

By introducing polar coordinates $x = \rho\cos\theta$ and $y = \rho\sin\theta$, these coefficients can be written

$$A_1 = \frac{1}{2}\cos^4\gamma, \quad A_2 = \frac{1}{2}\sin^4\gamma, \quad A_3 = \cos^2\gamma\sin^2\gamma,$$

$$A_4 = \rho^2 \cos^2\gamma \sin^2\gamma, \quad A_5 = \rho^2 \cos^2\gamma \sin^2\gamma \cos(2\theta), \quad A_6 = \rho^2 \cos^2\gamma \sin^2\gamma \sin(2\theta),$$
$$A_7 = 2\rho \cos^3\gamma \sin\gamma \cos\theta, \quad A_8 = 2\rho \cos^3\gamma \sin\gamma \sin\theta,$$
$$A_9 = 2\rho \cos\gamma \sin^3\gamma \cos\theta, \quad A_{10} = 2\rho \cos\gamma \sin^3\gamma \sin\theta, \tag{A.7}$$

where $\gamma \in [0, \pi/2]$, $\rho \in [0, 1]$ and $\theta \in [0, 2\pi\rangle$.

A.1 Symmetries of V_4

We note some symmetries of the *quartic* potential under the parametrization (A.2). They are conditional symmetries, where the potential is invariant with some "compensating" interchange of λs:

Symmetry I:

The interchange

$$y \leftrightarrow -y \quad \text{or} \quad \theta \leftrightarrow 2\pi - \theta \tag{A.8}$$

can be compensated by

$$\{\text{Im}\,\lambda_5,\ \text{Im}\,\lambda_6,\ \text{Im}\,\lambda_7\} \leftrightarrow \{-\text{Im}\,\lambda_5,\ -\text{Im}\,\lambda_6,\ -\text{Im}\,\lambda_7\} \tag{A.9}$$

This is of course nothing but the reality condition of the potential.

Symmetry II:

Under

$$\gamma \leftrightarrow \frac{\pi}{2} - \gamma \tag{A.10}$$

together with

$$\lambda_1 \leftrightarrow \lambda_2, \quad \text{and} \quad \lambda_6 \leftrightarrow \lambda_7 \tag{A.11}$$

the potential is invariant. This is the symmetry under the interchange $\Phi_1 \leftrightarrow \Phi_2$.

Symmetry III:

Under

$$(x, y) \leftrightarrow (-x, -y) \quad \text{or} \quad \theta \leftrightarrow \pi + \theta \mod 2\pi \tag{A.12}$$

together with

$$\{\lambda_6, \lambda_7\} \leftrightarrow \{-\lambda_6, -\lambda_7\} \tag{A.13}$$

the potential is invariant. This is related to the well-known Z_2 symmetry [2, 28].

Symmetry IV:

Under

$$(x, y) \leftrightarrow (y, x) \quad \text{or} \quad \theta \leftrightarrow \frac{\pi}{2} - \theta \mod 2\pi \tag{A.14}$$

together with

$$\mathrm{Re}\,\lambda_5 \leftrightarrow -\mathrm{Re}\,\lambda_5 \quad \text{and} \quad \{\mathrm{Re}\,\lambda_6, \mathrm{Re}\,\lambda_7\} \leftrightarrow \{\mathrm{Im}\,\lambda_6, \mathrm{Im}\,\lambda_7\} \tag{A.15}$$

the potential is invariant.

A.2 Stability

For the stability condition to be satisfied, V_4 must be positive for all combinations of $\gamma \in [0, \pi/2]$, $\rho \in [0, 1]$ and $\theta \in [0, 2\pi\rangle$. This is both a necessary and a sufficient condition. Whenever $\lambda_4 \leq 0$, the potential will have its global maximum and minimum when $\rho = 1$. Thus, it is sufficient to check that $V_4(\gamma, \theta; \rho = 1)$ satisfies stability when λ_4 is non-positive. In order to see this, we return to eqs. (A.5) and (A.6) and rewrite the potential as

$$V_4 = \lambda_4(x^2 + y^2)\cos^2\gamma \sin^2\gamma + h(x, y)$$

where $h(x, y)$ is a harmonic function. The maximum principle tells us that $h(x, y)$ will attain its global minimum at the boundary where $x^2 + y^2 = 1$ ($\rho = 1$). Whenever $\lambda_4 \leq 0$, the term $\lambda_4(x^2 + y^2)\cos^2\gamma \sin^2\gamma$ will also attain its minimum whenever $\rho = 1$, and so will V_4.

Some points from the parameter space give us some rather simple stability conditions. We now turn our attention towards these special points.

$\gamma = 0$ **or** $\gamma = \pi/2$

First we consider the boundary points $\gamma = 0$ and $\gamma = \pi/2$.

$$\begin{aligned} V_4(\gamma = 0) &= \frac{\lambda_1}{2} \\ V_4(\gamma = \pi/2) &= \frac{\lambda_2}{2} \end{aligned}$$

This leaves us with the "trivial" stability conditions of (3.20):

$$\lambda_1 > 0 \quad \text{and} \quad \lambda_2 > 0. \tag{A.16}$$

$\underline{\rho = 0}$

Considering the points where $\rho = 0$, we find that

$$V_4(\rho = 0) = \frac{\lambda_1}{2}\cos^4\gamma + \frac{\lambda_2}{2}\sin^4\gamma + \lambda_3\cos^2\gamma\sin^2\gamma. \tag{A.17}$$

Thus, we must require that

$$\lambda_3 > -\frac{1}{2}\left(\frac{\lambda_1}{\tan^2\gamma} + \lambda_2\tan^2\gamma\right). \tag{A.18}$$

The right-hand side has its minimum for $\tan^2\gamma = \sqrt{\lambda_1/\lambda_2}$, and we obtain the following necessary constraint on λ_3:

$$\lambda_3 > -\sqrt{\lambda_1\lambda_2}, \tag{A.19}$$

in agreement with [53].

A.3 The limit $\lambda_6 = \lambda_7 = 0$

It is instructive to consider the simple limit

$$\lambda_6 = \lambda_7 = 0 \tag{A.20}$$

Then the quartic part of the potential can be written

$$V_4 = \frac{\lambda_1}{2}\cos^4\gamma + \frac{\lambda_2}{2}\sin^4\gamma + [\lambda_3 + \rho^2(\lambda_4 + \mathrm{Re}\,\lambda_5\cos 2\theta + \mathrm{Im}\,\lambda_5\sin 2\theta)]\cos^2\gamma\sin^2\gamma \tag{A.21}$$

This expression has the same structure as (A.17), with

$$\lambda_3 \to \lambda_3 + \rho^2[\lambda_4 + \mathrm{Re}\,\lambda_5\cos 2\theta + \mathrm{Im}\,\lambda_5\sin 2\theta]. \tag{A.22}$$

Thus, the condition for stability can be adapted from (A.19), leading to:

$$\lambda_3 + \min[0, \lambda_4 - |\lambda_5|] > -\sqrt{\lambda_1\lambda_2}, \tag{A.23}$$

as obtained by [53]. However, we stress that this constraint only applies when $\lambda_6 = \lambda_7 = 0$.

Appendix B

The Higgs–vector-boson couplings can be extracted from the covariant derivatives:

$$
\begin{aligned}
&(D^\mu\Phi_1)^\dagger(D_\mu\Phi_1)+(D^\mu\Phi_2)^\dagger(D_\mu\Phi_2)\\
&=\frac{ig}{2\cos\theta_W}Z^\mu\{-\cos 2\theta_W(\varphi_1^-\partial_\mu\varphi_1^+-\varphi_1^+\partial_\mu\varphi_1^-+\varphi_2^-\partial_\mu\varphi_2^+-\varphi_2^+\partial_\mu\varphi_2^-)\\
&+i[\eta_1\partial_\mu\chi_1-\chi_1\partial_\mu\eta_1+\eta_2\partial_\mu\chi_2-\eta_2\partial_\mu\chi_2]\}\\
&-\tfrac{1}{2}igW^{\mu\dagger}[(\eta_1-i\chi_1)\partial_\mu\varphi_1^+-\partial_\mu(\eta_1-i\chi_1)\varphi_1^++(\eta_2-i\chi_2)\partial_\mu\varphi_2^+-\partial_\mu(\eta_2-i\chi_2)\varphi_2^+]\\
&+\tfrac{1}{2}igW^{\mu}[(\eta_1+i\chi_1)\partial_\mu\varphi_1^--\varphi_1^-\partial_\mu(\eta_1+i\chi_1)+(\eta_2+i\chi_2)\partial_\mu\varphi_2^--\varphi_2^-\partial_\mu(\eta_2+i\chi_2)]+\cdots
\end{aligned}
\tag{B.1}
$$

These Higgs fields have to be transformed into the physical basis:

$$
\eta_i=R_{ji}H_j,\quad i=1,2,3, \tag{B.2}
$$

with

$$
\begin{pmatrix}\varphi_1^\pm\\ \varphi_2^\pm\end{pmatrix}=\begin{pmatrix}\cos\beta & -\sin\beta\\ \sin\beta & \cos\beta\end{pmatrix}\begin{pmatrix}G^\pm\\ H^\pm\end{pmatrix},\quad \begin{pmatrix}\chi_1\\ \chi_2\end{pmatrix}=\begin{pmatrix}\cos\beta & -\sin\beta\\ \sin\beta & \cos\beta\end{pmatrix}\begin{pmatrix}G^0\\ \eta_3\end{pmatrix} \tag{B.3}
$$

With all momenta incoming (in an obvious notation), we find

$$
\begin{aligned}
ZH^+H^-:&\quad \frac{-ig\cos 2\theta_W}{2\cos\theta_W}(p_\mu^+-p_\mu^-),\\
ZG^+G^-:&\quad \frac{-ig\cos 2\theta_W}{2\cos\theta_W}(p_\mu^+-p_\mu^-),\\
ZH_jH_k:&\quad \frac{-g}{2\cos\theta_W}[(\sin\beta R_{j1}-\cos\beta R_{j2})R_{k3}-(\sin\beta R_{k1}-\cos\beta R_{k2})R_{j3}](p_\mu^j-p_\mu^k),\\
ZH_jG^0:&\quad \frac{g}{2\cos\theta_W}(\cos\beta R_{j1}+\sin\beta R_{j2})(p_\mu^j-p_\mu^0),
\end{aligned}
\tag{B.4}
$$

and

$$
\begin{aligned}
W^\pm H^\mp H_j:&\quad \frac{g}{2}[\pm i(\sin\beta R_{j1}-\cos\beta R_{j2})+R_{j3}](p_\mu^j-p_\mu^\mp),\\
W^\pm G^\mp H_j:&\quad \frac{\mp ig}{2}(\cos\beta R_{j1}+\sin\beta R_{j2})(p_\mu^j-p_\mu^\mp),\\
W^\pm G^\mp G^0:&\quad \frac{g}{2}(p_\mu^0-p_\mu^\mp)
\end{aligned}
\tag{B.5}
$$

There are no $ZH^\pm G^\mp$ or $W^\pm H^\mp G^0$ couplings. The CP-conserving limit is obtained by evaluating R for $\alpha_2=0$, $\alpha_3=0$, $\alpha_1=\alpha+\pi/2$, with the mapping $H_1\to h$, $H_2\to -H$ and $H_3\to A$. In that limit, we recover the results of [10].

References

[1] T. D. Lee, Phys. Rev. D **8** (1973) 1226.

[2] S. Weinberg, Phys. Rev. Lett. **37**, 657 (1976).

[3] G. C. Branco and M. N. Rebelo, Phys. Lett. B **160** (1985) 117;
J. Liu and L. Wolfenstein, Nucl. Phys. B **289** (1987) 1;
S. Weinberg, Phys. Rev. D **42** (1990) 860;
Y. L. Wu and L. Wolfenstein, Phys. Rev. Lett. **73** (1994) 1762 [arXiv:hep-ph/9409421].

[4] A. Riotto and M. Trodden, Ann. Rev. Nucl. Part. Sci. **49** (1999) 35 [arXiv:hep-ph/9901362].

[5] M. Dine and A. Kusenko, Rev. Mod. Phys. **76** (2004) 1 [arXiv:hep-ph/0303065].

[6] J. R. Ellis, Eur. Phys. J. C **34** (2004) 51.

[7] C. R. Schmidt and M. E. Peskin, Phys. Rev. Lett. **69** (1992) 410.
D. Atwood, A. Aeppli and A. Soni, Phys. Rev. Lett. **69** (1992) 2754.

[8] W. Bernreuther and A. Brandenburg, Phys. Rev. D **49** (1994) 4481 [arXiv:hep-ph/9312210]. W. Bernreuther, A. Brandenburg and M. Flesch, CERN-TH/98-390, PITHA 98/41, arXiv:hep-ph/9812387.

[9] D. Atwood, S. Bar-Shalom, G. Eilam and A. Soni, Phys. Rept. **347** (2001) 1 [arXiv:hep-ph/0006032];
W. Bernreuther, A. Brandenburg, Z. G. Si and P. Uwer, Phys. Rev. Lett. **87** (2001) 242002 [arXiv:hep-ph/0107086];
E. Accomando *et al.*, arXiv:hep-ph/0608079.

[10] J.F. Gunion, H.E. Haber, G. Kane, S. Dawson, *The Higgs Hunter's Guide* (Addison-Wesley, Reading, 1990).

[11] W. Khater and P. Osland, Nucl. Phys. B **661** (2003) 209 [arXiv:hep-ph/0302004].

[12] A. K. Grant, Phys. Rev. D **51** (1995) 207 [arXiv:hep-ph/9410267].

[13] S. Eidelman *et al.* [Particle Data Group], Phys. Lett. B **592** (2004) 1.

[14] P. Gambino and M. Misiak, Nucl. Phys. B **611** (2001) 338 [arXiv:hep-ph/0104034].

[15] S. Bertolini, Nucl. Phys. B **272** (1986) 77.

[16] M. Boonekamp, Eur. Phys. J. C **33** (2004) S720; P. Achard *et al.* [L3 Collaboration], Phys. Lett. B **583** (2004) 14 [arXiv:hep-ex/0402003]; J. Abdallah *et al.* [DELPHI Collaboration], Eur. Phys. J. C **38** (2004) 1 [arXiv:hep-ex/0410017].

[17] G. Abbiendi *et al.* [OPAL Collaboration], Eur. Phys. J. C **18** (2001) 425 [arXiv:hep-ex/0007040].

[18] J. Wess and B. Zumino, Nucl. Phys. B **70**, 39 (1974).

[19] P. Fayet and S. Ferrara, Phys. Rept. **32** (1977) 249.

[20] S. Dimopoulos and H. Georgi, Nucl. Phys. B **193** (1981) 150.

[21] H. P. Nilles, Phys. Rept. **110** (1984) 1.

[22] H. E. Haber and G. L. Kane, Phys. Rept. **117** (1985) 75.

[23] G. Abbiendi *et al.* [OPAL Collaboration], Eur. Phys. J. C **37** (2004) 49 [arXiv:hep-ex/0406057].

[24] R. A. Diaz, Ph.D. thesis, arXiv:hep-ph/0212237.

[25] K. Cheung and O. C. W. Kong, Phys. Rev. D **68** (2003) 053003 [arXiv:hep-ph/0302111].

[26] I. F. Ginzburg, M. Krawczyk and P. Osland, arXiv:hep-ph/0101208; Nucl. Instrum. Meth. A **472** (2001) 149 [arXiv:hep-ph/0101229]; arXiv:hep-ph/0211371.

[27] G. C. Branco, L. Lavoura, J. P. Silva, "CP Violation" (Oxford Univ. Press, 1999).

[28] S. L. Glashow and S. Weinberg, Phys. Rev. D **15** (1977) 1958.

[29] S. Davidson and H. E. Haber, Phys. Rev. D **72** (2005) 035004 [Erratum-ibid. D **72** (2005) 099902] [arXiv:hep-ph/0504050].

[30] I. F. Ginzburg and I. P. Ivanov, arXiv:hep-ph/0312374; Phys. Rev. D **72** (2005) 115010 [arXiv:hep-ph/0508020].

[31] A. Abulencia *et al.* [CDF Collaboration], arXiv:hep-ex/0510065; [CDF Collaboration], FERMILAB-PUB-05-485-E.

[32] A. G. Akeroyd, A. Arhrib and E. M. Naimi, Phys. Lett. B **490**, 119 (2000) [arXiv:hep-ph/0006035]; A. Arhrib, arXiv:hep-ph/0012353.

[33] S. Kanemura, T. Kubota and E. Takasugi, Phys. Lett. B **313** (1993) 155 [arXiv:hep-ph/9303263].

[34] L. F. Abbott, P. Sikivie and M. B. Wise, Phys. Rev. D **21** (1980) 1393.

[35] G. G. Athanasiu, P. J. Franzini and F. J. Gilman, Phys. Rev. D **32** (1985) 3010.

[36] S. L. Glashow and E. Jenkins, Phys. Lett. B **196** (1987) 233.

[37] C. Q. Geng and J. N. Ng, Phys. Rev. D **38** (1988) 2857 [Erratum-ibid. D **41** (1990) 1715].

[38] M. Misiak and M. Steinhauser, arXiv:hep-ph/0609241.

[39] D. A. Ross and M. J. G. Veltman, Nucl. Phys. B **95** (1975) 135; M. J. G. Veltman, Nucl. Phys. B **123** (1977) 89.

[40] M. B. Einhorn, D. R. T. Jones and M. J. G. Veltman, Nucl. Phys. B **191** (1981) 146.

[41] S. Schael *et al.*, ALEPH Collaboration and DELPHI Collaboration and L3 Collaboration and OPAL Collaboration and SLD Collaboration and LEP Electroweak Working Group and SLD Electroweak Group and SLD Heavy Flavour Group. CERN-PH-EP/2005-041; SLAC-R-774, Sep 2005, Phys. Rept. **427** (2006) 257; arXiv:hep-ex/0509008.

[42] D. Chang, W. F. Chang, C. H. Chou and W. Y. Keung, Phys. Rev. D **63** (2001) 091301 [arXiv:hep-ph/0009292].

[43] S. M. Barr and A. Zee, Phys. Rev. Lett. **65** (1990) 21 [Erratum-ibid. **65** (1990) 2920].

[44] S. de Jong, Plenary talk at EPS International Europhysics Conference on High Energy Physics (HEP-EPS 2005), Lisbon, Portugal, 21-27 July 2005; arXiv:hep-ex/0512043.

[45] G. W. Bennett *et al.* [Muon g-2 Collaboration], Phys. Rev. Lett. **92** (2004) 161802 [arXiv:hep-ex/0401008].

[46] A. Denner, R. J. Guth, W. Hollik and J. H. Kuhn, Z. Phys. C **51** (1991) 695.

[47] T. Hahn and M. Perez-Victoria, Comput. Phys. Commun. **118** (1999) 153 [arXiv:hep-ph/9807565]. See also http://www.feynarts.de/looptools/

[48] G. J. van Oldenborgh and J. A. Vermaseren, Z. Phys. C **46** (1990) 425.

[49] T. P. Cheng and M. Sher, Phys. Rev. D **35** (1987) 3484; M. Sher and Y. Yuan, Phys. Rev. D **44** (1991) 1461; M. Sher, in Proceedings of 29th International Conference on High-Energy Physics (ICHEP 98), Vancouver, Canada, 23-29 July 1998; arXiv:hep-ph/9809590.

[50] D. Atwood, L. Reina and A. Soni, Phys. Rev. D **55** (1997) 3156 [arXiv:hep-ph/9609279].

[51] A. C. Kraan [CDF - Run II Collaboration], arXiv:hep-ex/0611017.

[52] J. Pumplin, D. R. Stump, J. Huston, H. L. Lai, P. Nadolsky and W. K. Tung, JHEP **0207** (2002) 012 [arXiv:hep-ph/0201195].

[53] N. G. Deshpande and E. Ma, Phys. Rev. D **18** (1978) 2574.

[54] S. Nie and M. Sher, Phys. Lett. B **449** (1999) 89 [arXiv:hep-ph/9811234].

[55] S. Kanemura, T. Kasai and Y. Okada, Phys. Lett. B **471** (1999) 182 [arXiv:hep-ph/9903289].

[56] P. M. Ferreira, R. Santos and A. Barroso, Phys. Lett. B **603** (2004) 219 [Erratum-ibid. B **629** (2005) 114] [arXiv:hep-ph/0406231].